doi:10.1093/jmcb/mjaa056
Published online October 13, 2020

Article

LncRNA *Platr22* promotes super-enhancer activity and stem cell pluripotency

Pixi Yan[1,†], J. Yuyang Lu[1,†], Jing Niu[1], Juntao Gao[1], Michael Q. Zhang[1], Yafei Yin[1,2,*], and Xiaohua Shen[1,*]

[1] Tsinghua-Peking Joint Center for Life Sciences, School of Medicine and School of Life Sciences, Tsinghua University, Beijing, China
[2] Present address: Department of Cell Biology, Zhejiang University School of Medicine, Hangzhou, China
[†] These authors contributed equally to this work.
[*] Correspondence to: Yafei Yin, E-mail: yafei@tsinghua.edu.cn; Xiaohua Shen, E-mail: xshen@tsinhua.edu.cn

Edited by Zefeng Wang

Super-enhancers (SEs) comprise large clusters of enhancers, which are co-occupied by multiple lineage-specific and master transcription factors, and play pivotal roles in regulating gene expression and cell fate determination. However, it is still largely unknown whether and how SEs are regulated by the noncoding portion of the genome. Here, through genome-wide analysis, we found that long noncoding RNA (lncRNA) genes preferentially lie next to SEs. In mouse embryonic stem cells (mESCs), depletion of SE-associated lncRNA transcripts dysregulated the activity of their nearby SEs. Specifically, we revealed a critical regulatory role of the lncRNA gene *Platr22* in modulating the activity of a nearby SE and the expression of the nearby pluripotency regulator *ZFP281*. Through these regulatory events, *Platr22* contributes to pluripotency maintenance and proper differentiation of mESCs. Mechanistically, *Platr22* transcripts coat chromatin near the SE region and interact with DDX5 and hnRNP-L. DDX5 further recruits p300 and other factors related to active transcription. We propose that these factors assemble into a transcription hub, thus promoting an open and active epigenetic chromatin state. Our study highlights an unanticipated role for a class of lncRNAs in epigenetically controlling the activity and vulnerability to perturbation of nearby SEs for cell fate determination.

Keywords: lncRNA, *Platr22*, super-enhancer, pluripotency

Introduction

Enhancers are *cis*-regulatory DNA regions that positively control the activity of promoters in a cell type- or tissue-specific manner (Andersson et al., 2014; Li et al., 2016). These regions, which comprise multiple binding sites for combinations of transcription factors and coactivators, provide a platform for facilitating the recruitment of RNA polymerase II and other regulators that are necessary for target gene activation (Ong and Corces, 2011; Rickels and Shilatifard, 2018). Super-enhancers (SEs), which consist of clusters of enhancers and harbor an unusually high density of transcription factors and mediator coactivators, play a key role in the control of cell identity and disease (Hnisz et al., 2013; Whyte et al., 2013). Compared to typical enhancers (TEs), SEs are usually longer, harbor more bound transcription factors, and have higher expression of enhancer RNA (eRNA; SEs vs. TEs, ~10-fold), an indicator enhancer activity (Hnisz et al., 2013; Lovén et al., 2013; Whyte et al., 2013; ZHu et al., 2013). Several studies have shown that deletion or mutations of SEs can downregulate the expression levels of target genes in specific cell lines. For instance, deleting the distal SE of *Sox2* reduces the expression of *Sox2* by over 90%, and genomic editing of SEs reveals functional hierarchy of SE, which contributes to the lineage and stage-specific transcription during hematopoiesis (Li et al., 2014a; Huang et al., 2016).

Most SEs express RNAs (seRNAs), e.g. in macrophages, 93.3% of SEs express seRNAs (Hah et al., 2015). Moreover, it was reported that the stage-specific transcription of seRNAs might be involved in cardiac-related functions by regulating co-expressed genes, which suggests that seRNAs may play a key role in the function of their SEs (Chang et al., 2019). SEs and their associated seRNAs function as a type of molecular rheostat to control gene expression (Andersson et al., 2014; Hah et al., 2015). Although the function of SEs and seRNAs are well characterized, the regulation of SE activity, especially the

Received May 27, 2020. Revised August 17, 2020. Accepted September 14, 2020.

mechanism by which the nearby *cis* noncoding sequences regulate the activity of SEs, remains largely unknown.

In mammalian genomes, >80% of the DNA is transcribed, even though only 2% consists of protein-coding genes (Djebali et al., 2012). This prevalent transcription produces thousands of long noncoding RNAs (lncRNAs). Compared to protein-coding mRNAs, lncRNAs are less conserved, are expressed at a low level, and tend to be retained in the nucleus where they are associated with chromatin (Derrien et al., 2012; Tilgner et al., 2012; Yin et al., 2020). The chromatin association of lncRNA is correlated with its function in modulating the expression and processing of nearby genes (Yan et al., 2017; Sun et al., 2018). For example, *Haunt*, a lncRNA located ~40 kb upstream of the *HOXA* gene cluster, specifically targets *HOXA* loci to modulate the expression of *HOXA* gene during retinoic acid-induced differentiation (Yin et al., 2015).

Similar to the activity of SEs, the expression of lncRNA exhibits strong spatial and temporal specificity, which implies that potential regulatory or functional linkages may exist between these SEs and lncRNAs. Studies of several individual lncRNA genes that overlap with or neighbor SEs suggest that SE-associated lncRNA (SE-lncRNA) genes and/or transcripts may play roles in some cellular processes (Sauvageau et al., 2013; Xiang et al., 2014; Ounzain et al., 2015; Micheletti et al., 2017). For instance, the lncRNA *CCAT1-L*, which is transcribed specifically in human colorectal cancers from a locus 515 kb upstream of *MYC*, facilitates chromatin looping between the *MYC* promoter and a nearby SE, thereby promoting *MYC* expression (Xiang et al., 2014). Despite these individual cases, a general linkage between SEs and lncRNAs is still missing, and the biological roles of lncRNAs in SE function and the underlying mechanism remain to be solved.

Here, through comprehensive locus characterization, we revealed a pattern of juxtaposition between lncRNA genes and SEs in the genome. Remarkably, knockdown (KD) of 8 out of 9 SE-lncRNA genes dysregulated the activity of their nearby SEs, which indicates that SE-lncRNAs regulate the activity of nearby SEs. We then focused on the lncRNA *Platr22* (pluripotency-associated transcript 22) and performed in-depth characterization of its regulatory effects on its nearby SE (^{Platr22}SE) via complementary approaches in mouse embryonic stem cells (mESCs). *Platr22* is required for the activity of ^{Platr22}SE and the expression of its upstream gene *ZFP281*, a key pluripotency regulator in mESCs. Depletion of *Platr22* impairs the expression of pluripotency genes and proper ESC differentiation. Mechanistically, *Platr22* RNA transcripts, the ^{Platr22}SE DNA locus, and the *ZFP281* genomic region interact with each other to create a transcriptional hub. *Platr22* modulates the activity of the hub through interaction with hnRNP-L and DDX5, which further recruit p300 and promote an open and active epigenetic state and ^{Platr22}SE activity. Our results demonstrate that SE-lncRNAs, or at least a subset of them, *cis*-regulate the activity and vulnerability to perturbation of nearby SEs and are involved in processes such as establishment of diverse cell identities and cell fate decision.

Results

Genomic juxtaposition of SEs with lncRNAs

In an effort to reveal the potential link between lncRNA genes and SEs, we compared the genomic distribution patterns between lncRNA genes and SEs in mESCs. We first identified all genes positioned next to SEs and TEs (within 200 kb) and compared them to randomly picked genomic regions. For lncRNA genes that lie next to SEs, the distribution pattern showed a peak at 10 kb and was 2- to 3-fold higher than the genomic background (Figure 1A). In contrast, for lncRNA genes next to a TE, the distribution was much flatter, with a 1.3- to 1.8-fold enrichment over the background. These results suggest that SEs tend to be located close to lncRNA genes (Figure 1A). In comparison, protein-coding mRNA genes are more likely to be further away from SEs than from TEs. Protein-coding genes positioned within 20 kb of an enhancer are more likely to be associated with a TE than an SE (coding-TE vs. coding-SE; $P = 0.038$, *t*-test), while protein-coding genes located in the range of 20–180 kb from an enhancer are more likely to be associated with an SE than a TE (coding-SE vs. coding-E, $P = 8.6 \times 10^{-27}$, *t*-test) (Figure 1A). In addition, compared to TEs, a substantially larger proportion of SEs overlap with at least one lncRNA gene in the genome (29% for TEs vs. 58% for SEs, $P = 1.2 \times 10^{-19}$) (Figure 1B). In comparison, protein-coding genes are not preferentially located next to SEs or TEs, and SEs are significantly more likely to be next to a lncRNA gene than a coding gene (58% vs. 46%, $P = 2.8 \times 10^{-34}$) (Figure 1B; Supplementary Figure S1A). These results indicate that lncRNA genes tend to be in juxtaposition with SEs in mESCs.

To ask whether the connection between SEs and lncRNA genes is a general phenomenon, we expanded the analysis to 20 mouse and 86 human tissues and cell lines. Strikingly, in all of the 20 mouse and 82 out of 86 human tissues/cell lines analyzed, SEs showed a significantly higher tendency to be in juxtaposition with lncRNA genes than with protein-coding mRNA genes ($P < 0.05$) (Supplementary Figure S1B). Notably, compared to TE-associated lncRNA (TE-lncRNA) genes, SE-lncRNA genes harbor higher cell-type specificity (53% vs. 32% in one cell type) (Figure 1C; Supplementary Figure S1C, D and Table S1). Moreover, lncRNA genes that overlap with SEs in the genome are more conserved and substantially older than TE-lncRNA genes and other lncRNA genes (median evolutionary age: 4.6 vs. 4.9 vs. 5.5, $P < 0.0283$, Wilcoxon test) in mouse (Supplementary Figure S1E). Taken together, these results suggest that SEs and lncRNA genes tend to be juxtaposed with each other, which implies a biological link between them.

SE-lncRNA genes regulate the activity of nearby SEs

To investigate the potential regulatory role of SE-lncRNA genes, we chose lncRNA genes that are located <20 kb from

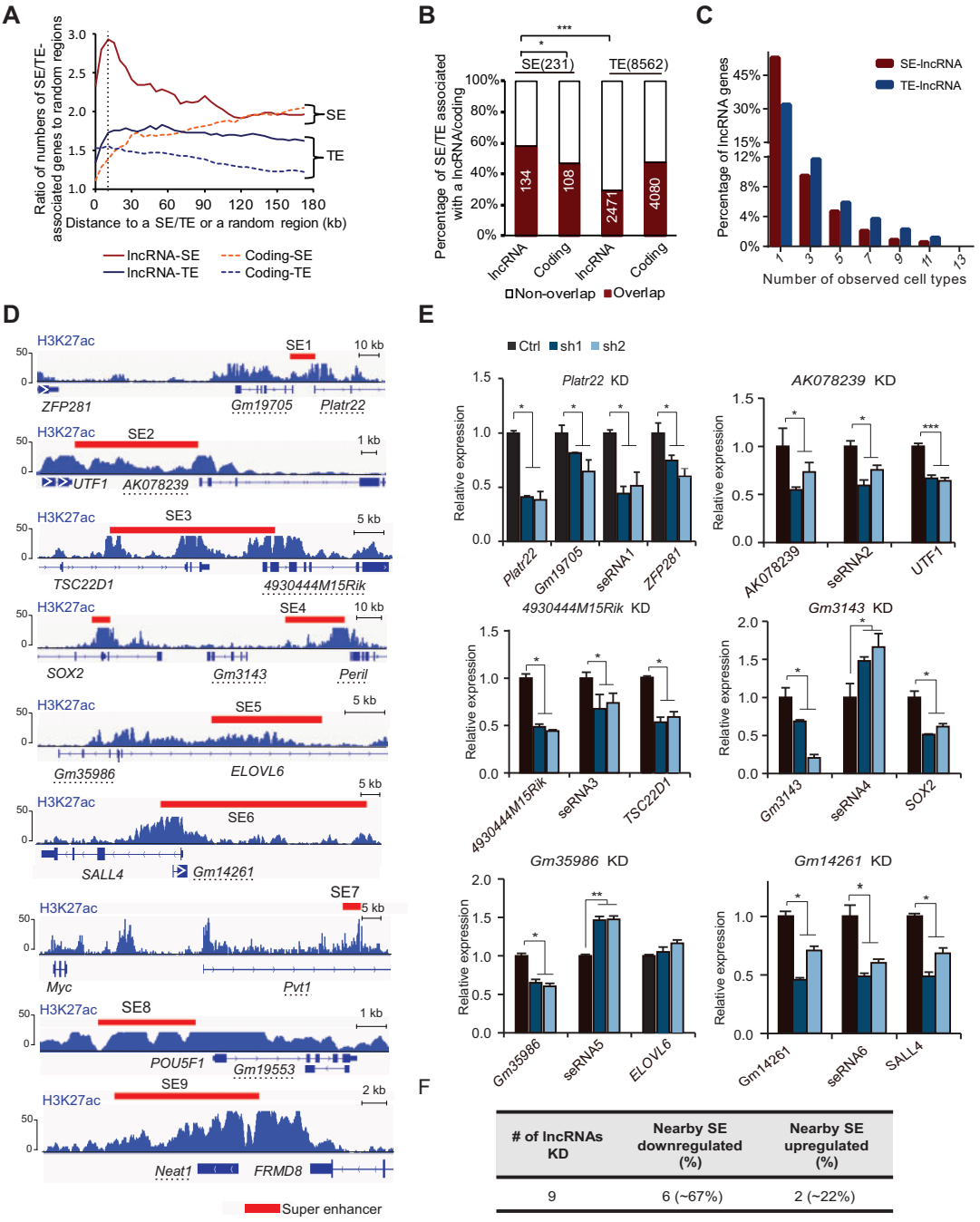

# of lncRNAs KD	Nearby SE downregulated (%)	Nearby SE upregulated (%)
9	6 (~67%)	2 (~22%)

Figure 1 Genomic juxtaposition of SEs and lncRNAs. (**A**) Ratio of SE/TE-associated gene numbers to the background in ESCs. The x-axis shows different genomic distance cutoffs for the definition of SE/TE-associated genes. The y-axis shows the ratio of numbers of SE/TE-associated genes to random genomic regions. (**B**) Bar plots showing a comparison of overlap patterns of SEs/TEs and coding/lncRNA genes in ESCs. The y-axis indicates the percentage of SEs/TEs that are overlapping or non-overlapping with a specific group of genes. Absolute enhancer numbers in each category are shown inside the bars. Fisher's exact test was conducted to evaluate the statistical difference between categories. $*P < 0.05$, $***P < 0.001$. (**C**) Specificity of SE-lncRNA and TE-lncRNA pairs. The y-axis indicates the percentage of lncRNA genes and the x-axis indicates the number of observed cell types with SE-lncRNA and TE-lncRNA pairs. (**D**) Nine examples of genomic regions containing SEs that are active in mESCs and nearby lncRNA genes. SEs are indicated as red boxes. H3K27ac histone modification patterns and corresponding scales are also shown. (**E**) The lncRNAs in **D** were knocked down, and the levels of the transcripts (from coding genes, lncRNA genes, and SEs) in each genomic region were determined. The y-axis represents relative mean expression normalized to *GAPDH* and the scramble shRNA (Ctrl). Data are shown as mean ± SD ($n = 4$, including two technical repeats for two independent KD experiments). $*P < 0.05$, $**P < 0.01$. (**F**) Statistical summary of the lncRNA genes and SEs analyzed by RNAi.

the nearest SE for further study. We designated this group of lncRNA genes as SE-lncRNA genes. We chose 9 SE-lncRNA genes from mESCs based on their expression (Whyte et al., 2013; Yin et al., 2015). Six of the lncRNA genes are overlapped with or located within 1 kb from the nearest SEs (*Platr22*, *4930444M15Rik*, *Gm14261*, *Neat1*, *AK078239*, and *Pvt1*), and the other three lncRNA genes are located within 20 kb from the nearest SEs (*Gm35986*, *Gm3143*, and *Gm19553*) (Figure 1D). Similar to previously reported lncRNA features (Clark et al., 2012; Yin et al., 2020), all of these nine SE-lncRNA genes are moderately processed, and the majority of their RNA transcripts are located in chromatin fraction (Supplementary Figure S1F and G). The adjacent protein-coding genes of some of these SE-lncRNA genes, including *ZFP281*, *UTF1*, *SOX2*, and *MYC*, were reported to play key roles in mESC pluripotency maintenance and differentiation (Okuda et al., 1998; Fong et al., 2008; Fidalgo et al., 2011, 2016; Chappell and Dalton, 2013). We performed shRNA KD to attenuate the expression of these nine lncRNA transcripts and analyzed the activity of their nearby SEs by RT-qPCR detection of eRNA. Strikingly, depletion of eight out of these nine (89%) lncRNA transcripts dysregulated the activity of their nearby SEs. Among them, six impaired while two enhanced the activity of the SE (Figure 1E; Supplementary Figure S1F). Moreover, depleting six SE-lncRNAs also impaired the expression of the nearest protein-coding genes (Figure 1E; Supplementary Figure S1F). This result suggests that SE-lncRNAs modulate the activity of their nearby SEs and the expression of their nearby genes, which may be a prevalent phenomenon.

Characterization of the SE-lncRNA Platr22

In order to dissect the molecular function of SE-lncRNA genes and the mechanism by which they regulate their associated SEs, we focused our study on a locus containing a SE-lncRNA gene, *Platr22*, which partially overlaps with a SE, designated as ^{Platr22}SE. This locus is located ~53 kb downstream of *ZFP281* (Figures 1D and 2A). *ZFP281* encodes a Krüppel-like zinc finger transcription factor, which was reported to play a key role in mouse early embryonic development, and directly regulates the expression of genes related to pluripotency and development (Fidalgo et al., 2012; Huang et al., 2017). Interestingly, *ZFP281* controls pluripotency in a dosage-dependent manner via both transcriptional activation and repression (Wang et al., 2008; Fidalgo et al., 2011; 2016). The *Platr22* gene locus, together with ^{Platr22}SE itself, is enriched with ChIP-seq signals of active histone markers like H3K4me3, H3K4me1, and H3K27ac, as well as transcription regulators like *ZFP281*, *SOX2*, *P300*, etc. (Figure 2A; Supplementary Figure S2A). Notably, the ^{Platr22}SE-*Platr22* pair is positionally conserved between human and mouse (Supplementary Figure S2B). We conducted a rapid amplification of cDNA ends assay and confirmed that ^{Platr22}seRNA was not an extended transcript of *Platr22* or another lncRNA, *Gm19705*, which is located upstream of the SE (Supplementary Figure S2C). Interestingly, GRO-seq analysis suggested that the *Platr22* gene generates the highest GRO-seq signal in this region, even when compared with the *ZFP281* gene (Figure 2A).

Subcellular fractionation assays indicated that ~84% of *Platr22* transcripts are associated with chromatin (Figure 2B). RNA fluorescence *in situ* hybridization (FISH) of *Platr22* transcripts in mESCs detected one or two foci in the nucleus (Figure 2C), which implies that *Platr22* RNA transcripts are mainly associated with their own nearby genomic locus. To further reveal the DNA target of *Platr22* transcripts, we performed chromatin isolation by RNA purification (ChIRP) of endogenous *Platr22* transcripts (Figure 2D; Chu et al., 2011; Yin et al., 2015). ChIRP-seq indicated that *Platr22* transcripts mainly bound to their own locus and spread to the downstream ~120 kb and upstream ~50 kb region, which includes the *ZFP281* DNA locus (Figure 2A and E). Strong ChIRP-seq signals were detected covering the whole ^{Platr22}SE region (Figure 2A, D, and E). As an alternative approach, we also analyzed the RNA–DNA interaction data generated by global RNA interactions with DNA by deep sequencing (GRID-seq) (Li et al., 2017b), which is an unbiased method for detecting global RNA–DNA interactions in mESCs. This further confirmed the binding of *Platr22* transcripts to the nearby loci (Figure 2A).

The RNA FISH and ChIRP-seq results imply that the *Platr22* gene locus and the *ZFP281* gene locus may be closely adjacent to each other in the higher order chromatin structure. Indeed, by analyzing data generated from high-throughput chromosome conformation capture (Hi-C), we found the ^{Platr22}SE, the *Platr22* gene, and the *ZFP281* locus are located in the same 'topologically associating domains' (Figure 2A; Dixon et al., 2012). SEs, seRNAs, and transcription factors are reportedly located in the same 'super enhancer domain' (SE domain), which can act as a functional module to regulate transcriptional networks (Hah et al., 2015). Interestingly, the *Platr22*, *Gm19705*, ^{Platr22}SE, and *ZFP281* loci are all located in the same SE domain. Moreover, chromatin interaction maps generated by both paired-end tagging (ChIA-PET) of RNA Pol II and promoter capture Hi-C suggested that the ^{Platr22}SE locus interacts with the promoter region of *ZFP281* (Zhang et al., 2013; Novo et al., 2018). We further performed chromatin conformation capture (3C) in wild-type (WT) mESCs, which further confirmed the ^{Platr22}SE and the promoter of *ZFP281* loci were positioned in close proximity on chromatin (Supplementary Figure S2E). Taken together, these results suggest that *Platr22* RNA transcripts mainly bind to their own coding region and associate with the ^{Platr22}SE locus. The ^{Platr22}SE locus and *Platr22* RNA transcripts create an interactive hub that the *ZFP281* DNA locus can interact with, and these three loci are closely associated with each other.

Platr22 regulates the activity of ^{Platr22}SE and the expression of ZFP281

Our initial shRNA KD screen showed that *Platr22* depletion impairs the expression of ^{Platr22}seRNA and *ZFP281* (Figure 1E).

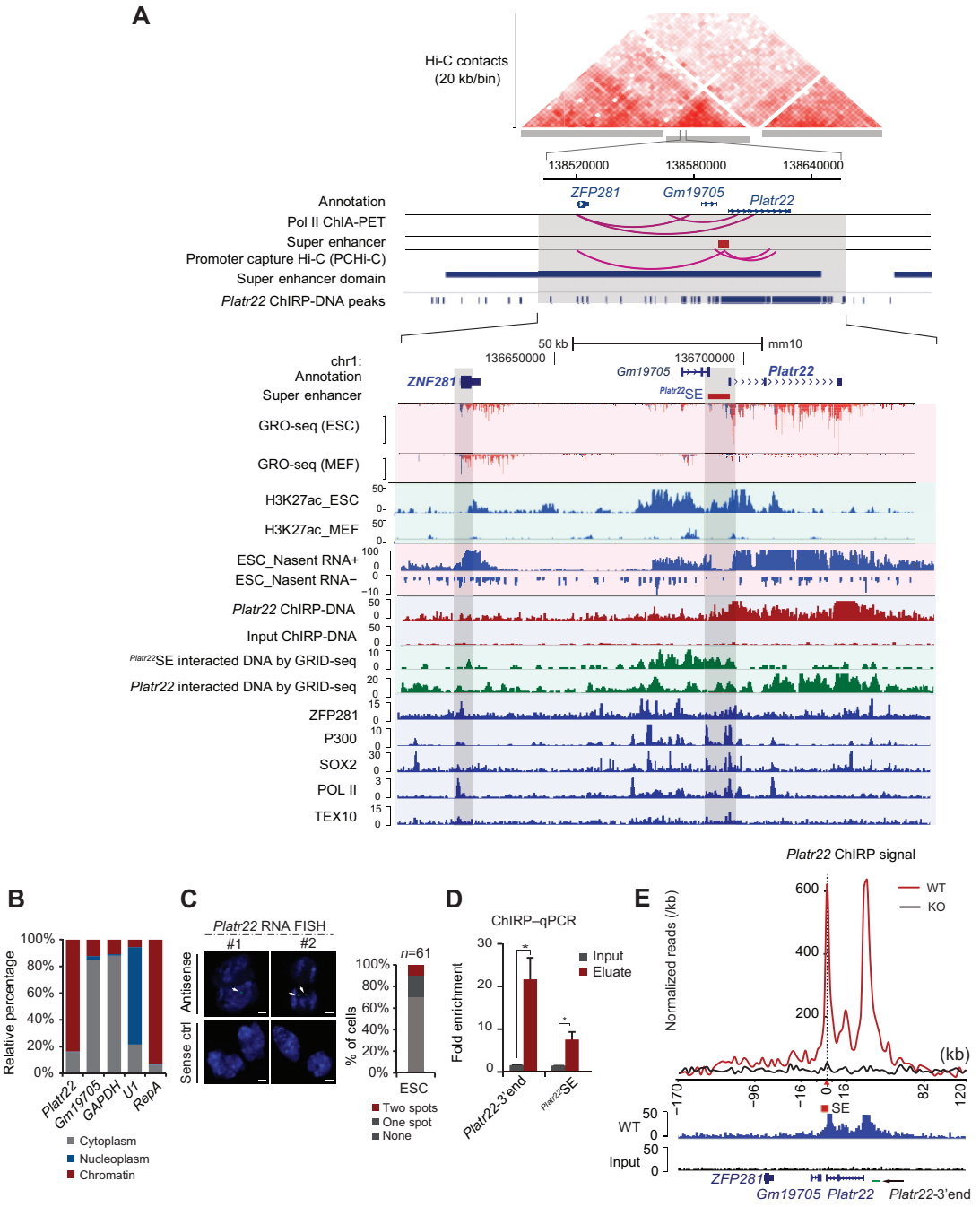

Figure 2 *Platr22* positively regulates nearby SE activity. (**A**) The ^{Platr22}SE and the *Platr22* locus on chromosome 1 in the genome browser. The topological domain and looping structure indicated by Hi-C contacts and Pol II ChIA-PET are shown. The upper tracks show *Platr22* ChIRP-DNA peaks and the region containing the SE domain in ESCs. Tracks below show signals of *Platr22* GRO-seq (blue, transcribed from negative-strand; red, transcribed from positive-strand), ChIRP-DNA, *Platr22* GRID-seq, ^{Platr22}SE GRID-seq, DNase I hypersensitivity, and ChIP-seq in ESCs. The SE region near *Platr22* and the promoter region of *ZFP281* are boxed in light gray. (**B**) Subcellular fractionation of *Platr22* and *Gm19705* transcripts. *GAPDH*, *U1*, and *RepA* RNAs serve as controls for the cytosolic, nuclear, and chromatin fractions, respectively. (**C**) *Platr22* RNA FISH in ESCs. *Platr22*-sense RNA probes (bottom) serve as controls. Scale bar, 10 μm. A statistical summary is shown (right panel). Light gray, dark gray, and red boxes represent ESCs with 0, 1, and 2 *Platr22* spots, respectively. The numbers of cells analyzed are indicated. (**D**) ChIRP analysis of chromatin occupancy by *Platr22* RNA. The y-axis shows fold enrichment to input of ChIRP signals in ESCs. Data are shown as mean ± SD ($n = 4$, including two technical repeats for two independent biological replicates). *$P < 0.05$. (**E**) A zoomed-out view of *Platr22* ChIRP DNA-seq signals in WT ESCs within a 290-kb range of the *Platr22* locus. The red arrow shows the TSS of *Platr22*. Normalization was performed by dividing the number of actual reads in each 10-kb bin by sequencing depth. The ChIRP DNA-seq tracks of *Platr22* are shown (bottom).

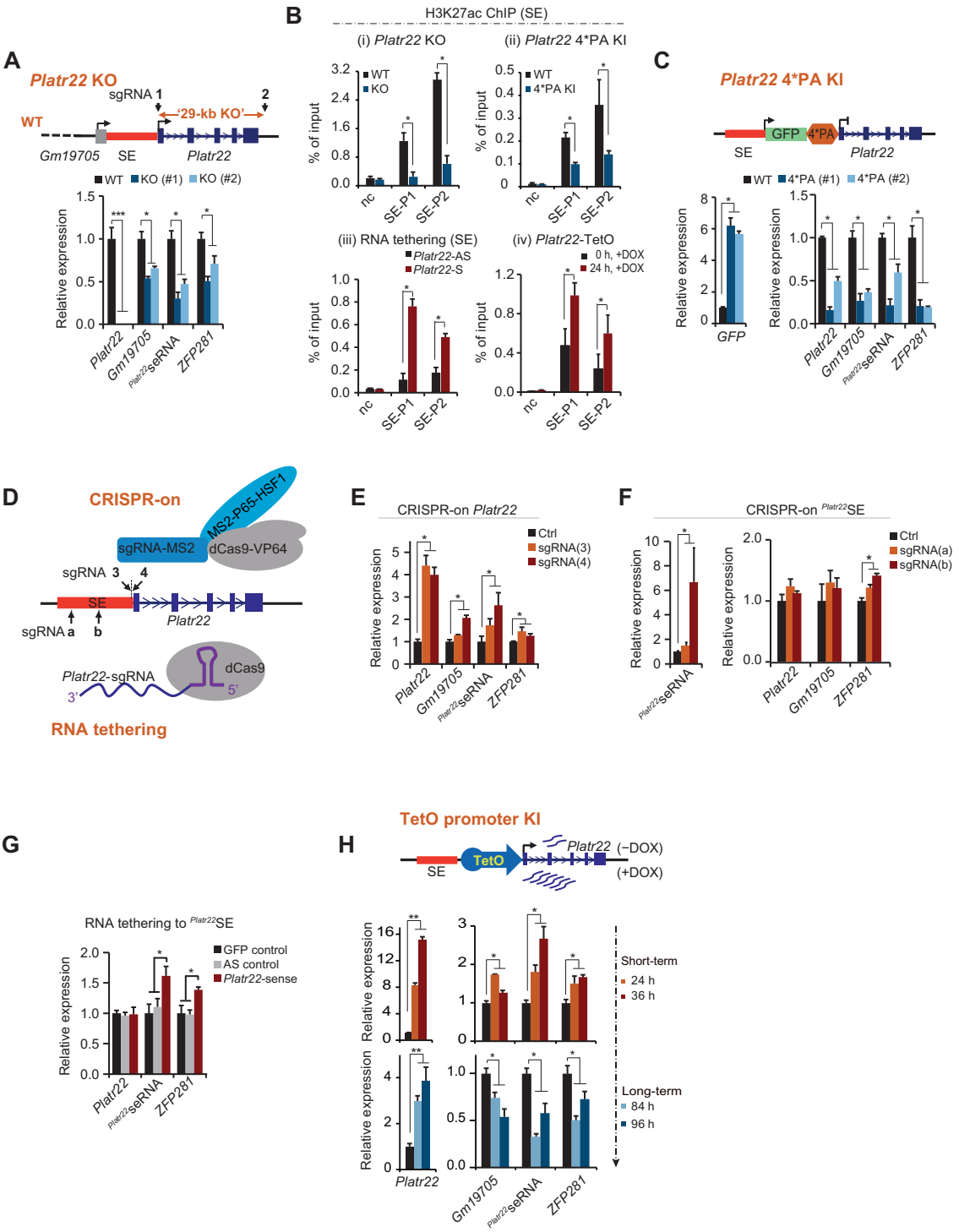

Figure 3 *Platr22* regulates the transcriptional activity of ^{Platr22}SE. (**A**) Schematic diagram of *Platr22* KO (upper). RT-qPCR analysis in *Platr22* KO ESCs (bottom). (**B**) ChIP–qPCR of H3K27ac on ^{Platr22}SE in *Platr22* KO cells (i), *Platr22* 4*PA KI cells (ii), cells with tethering of *Platr22* RNA (iii), and *Platr22*-TetO KI cells with 24 h DOX treatment (iv). The y-axis shows the percentages of input. 'nc' shows an unrelated region ('nc', primer CSa). SE-P1, primer 1 in ^{Platr22}SE region; SE-P2, primer 2 in ^{Platr22}SE region. (**C**) Schematic diagram of GFP-4*PA KI (upper). RT-qPCR analysis in GFP-4*PA KI ESCs (bottom). (**D**) Upper: schematic diagram of CRISPR/Cas9-mediated activation (CRISPR-on) of *Platr22* and ^{Platr22}SE. sgRNA 3 and sgRNA 4 target the promoter of *Platr22*, and sgRNA a and sgRNA b target the SE region. Bottom: schematic diagram of CRISPR/dCas9-mediated RNA tethering. sgRNAs are shown. (**E** and **F**) RT-qPCR analysis of relative gene expression levels during CRISPR-on of *Platr22* and ^{Platr22}SE. (**G**) RT-qPCR analysis of the effect of tethering *Platr22* transcripts to the nearby ^{Platr22}SE region. *Platr22*-sense transcript, *Platr22*-antisense transcript (AS), or GFP RNA was fused with an sgRNA targeting the ^{Platr22}SE region. (**H**) Schematic diagram of TetO promoter KI in the TSS of *Platr22* in ESCs (upper). RT-qPCR analysis in *Platr22*-TetO KI ESCs at 0, 24, 36, 84, and 96 h upon DOX treatment. Expression (y-axis) was normalized to *GAPDH* and then fold change was calculated relative to 0 h. All data are shown as mean ± SD ($n = 4$, including two technical repeats for two independent biological replicates). *$P < 0.05$, **$P < 0.01$.

To further validate this result, we sought to use alternative strategies to characterize the regulatory role of *Platr22* transcripts toward these two loci. First, we conducted CRISPR/Cas9-mediated knockout (KO) to delete a ~29-kb region covering the whole genomic region of *Platr22* (*Platr22* KO) (Figure 3A; Supplementary S3A and B). Consistent with the RNA interference (RNAi) data, the expression of ^{Platr22}seRNA, *ZFP281*, and *Gm19705* were substantially downregulated in *Platr22* KO cells (Figure 3A). Moreover, the level of H3K27ac, an indicator of active enhancers, is also decreased at the ^{Platr22}seRNA locus (Figure 3B (i)), which further supports the notion that the activity of ^{Platr22}SE is decreased in the absence of the *Platr22* locus.

CRISPR/Cas9-mediated *Platr22* KO may delete potential regulatory DNA elements embedded in the *Platr22* genomic region, as well as remove *Platr22* RNA transcripts (Yin et al., 2015). To dissect the function of *Platr22* RNA transcripts from the *Platr22* genomic region and transcription *per se*, we inserted a cassette comprising GFP fused with a 4×polyA stop signal (GFP-4*PA) immediately downstream of the *Platr22* transcription start site (TSS) (Figure 3C; Supplementary Figure S3C and D). In GFP-4*PA knockin (KI) cells, the expression of *Platr22* transcripts was reduced by 50%–90%, while the GFP RNA level increased by 7-fold (Figure 3C; Supplementary Figure S3E). Similar to shRNA KD and *Platr22* KO, GFP-4*PA KI also caused substantial downregulation of the expression of *ZFP281*, *Gm19705*, and ^{Platr22}seRNA (Figure 3C). In addition, the level of H3K27ac is also decreased at the ^{Platr22}seRNA locus in GFP-4*PA KI mESCs (Figure 3B (ii)). This result suggests that the regulatory effect of the *Platr22* locus is exerted mainly through *Platr22* RNA transcripts.

Next, we studied the effect of overexpressing *Platr22* transcripts on ^{Platr22}seRNA and *ZFP281*. Ectopic expression of *Platr22* transcripts by plasmid transfection failed to alter the expression of ^{Platr22}seRNA, *ZFP281*, and *Gm19705* (Supplementary Figure S3F). However, *in situ* overexpression of *Platr22* transcripts through the CRISPR-on system (Konermann et al., 2015) substantially increased the expression of *ZFP281*, ^{Platr22}seRNA, and *Gm19705* by 1.5- to 2.5-fold (Figure 3D and E). CRISPR-on with sgRNAs targeting the ^{Platr22}seRNA region increased the expression of ^{Platr22}SE by 1.5- to 7-fold and elevated *ZFP281* expression by 1.2- to 1.4-fold, while it failed to affect *Platr22* expression (Figure 3F). This suggests that *Platr22* functions upstream of ^{Platr22}SE. Moreover, by using the CRISPR/Cas9 system to guide and tether ectopically expressed *Platr22* transcripts to the ^{Platr22}SE region, we found that sense RNA transcripts, but not control antisense transcripts, substantially increased the expression of *ZFP281* and the activity of ^{Platr22}SE (Figure 3B (iii) and G; Shechner et al., 2015). These results further support the notion that *Platr22* modulates the expression of *ZFP281* and the activity of ^{Platr22}SE through its RNA transcripts.

To assess the regulatory effect of *Platr22* transcripts on ^{Platr22}SE and *ZFP281* in an inducible way, we inserted a tetracycline-inducible promoter (TetO promoter KI) immediately upstream of the *Platr22* TSS (*Platr22*-TetO) (Figure 3H; Supplementary S3G and H). Upon short-term (24 and 36 h) doxycycline (DOX) treatment, *Platr22* expression was elevated by 8- to 16-fold in TetO KI mESCs. Accordingly, the expression of *ZFP281* and the activity of ^{Platr22}SE were substantially elevated (Figure 3B (iv) and H). Surprisingly, prolonged DOX treatment (long-term, 84 and 96 h) in *Platr22*-TetO mESCs still upregulated the expression of *Platr22* by 3- to 4-fold, while the expression of ^{Platr22}seRNA and *ZFP281* was reduced by 30%–60% (Figure 3H). This result suggests that persistent high-level expression of *Platr22* transcripts attenuated ^{Platr22}SE activity, which indicates that a precise balance of *Platr22* expression is required for proper ^{Platr22}SE activity.

Platr22 contributes to mESC pluripotency maintenance through regulation of ZFP281 expression

To investigate the molecular defects that occur upon depletion of *Platr22* transcripts in mESCs, we performed RNA-seq analyses of WT and KO/4*PA KI mESCs (Supplementary Figure S4A and Table S2). As the KO cells may also lack potential regulatory DNA elements embedded in the *Platr22* genomic region, we mainly focused our study on 4*PA KI mESCs, which have minimal disruption of the *Platr22* genomic DNA. Compared to WT cells, depletion of *Platr22* transcripts by 4*PA KI downregulated the expression of 941 genes and upregulated 907 genes (fold change >1.5, $P<0.05$; Figure 4A). For most of these dysregulated genes, similar expression level changes were also observed in *Platr22* KO mESCs (Figure 4A). Notably, gene ontology (GO) analysis indicates that these dysregulated genes are substantially enriched in developmental process-related terms (Supplementary Figure S4B).

To investigate whether the dysregulation of developmental genes upon depletion of *Platr22* transcripts was caused by the downregulation of *ZFP281*, we compared our RNA-seq data with a previously reported RNA-seq dataset from *ZFP281* KO mESCs. Approximately 40% of downregulated genes in *Platr22* 4*PA KI mESCs are also downregulated in *ZFP281* KO cells, and the overlap is highly significant ($P=6.18\text{E}{-18}$; Figure 4B). Moreover, the set of overlapping genes is also enriched in developmental processes (Supplementary Figure S4C). This result, together with the observation that *Platr22* transcripts mainly bind to their own genomic locus (Figure 2C–E), suggests that *Platr22* functions by regulating the expression of *ZFP281*.

Interestingly, consistent with the TetO-induced overexpression of *Platr22* transcripts (Figure 3H), short-term *ZFP281* KD downregulated the expression of *Platr22*, *Gm19705*, and ^{Platr22}SE, while long-term *ZFP281* depletion upregulated their expression (Figure 4C). These findings are consistent with a previously reported dosage-dependent transcriptional regulation function of *ZFP281* (Wang et al., 2008; Fidalgo et al., 2011, 2016). Taken together, these results demonstrate that *Platr22* regulates mESC pluripotency mainly through modulating the expression of *ZFP281*.

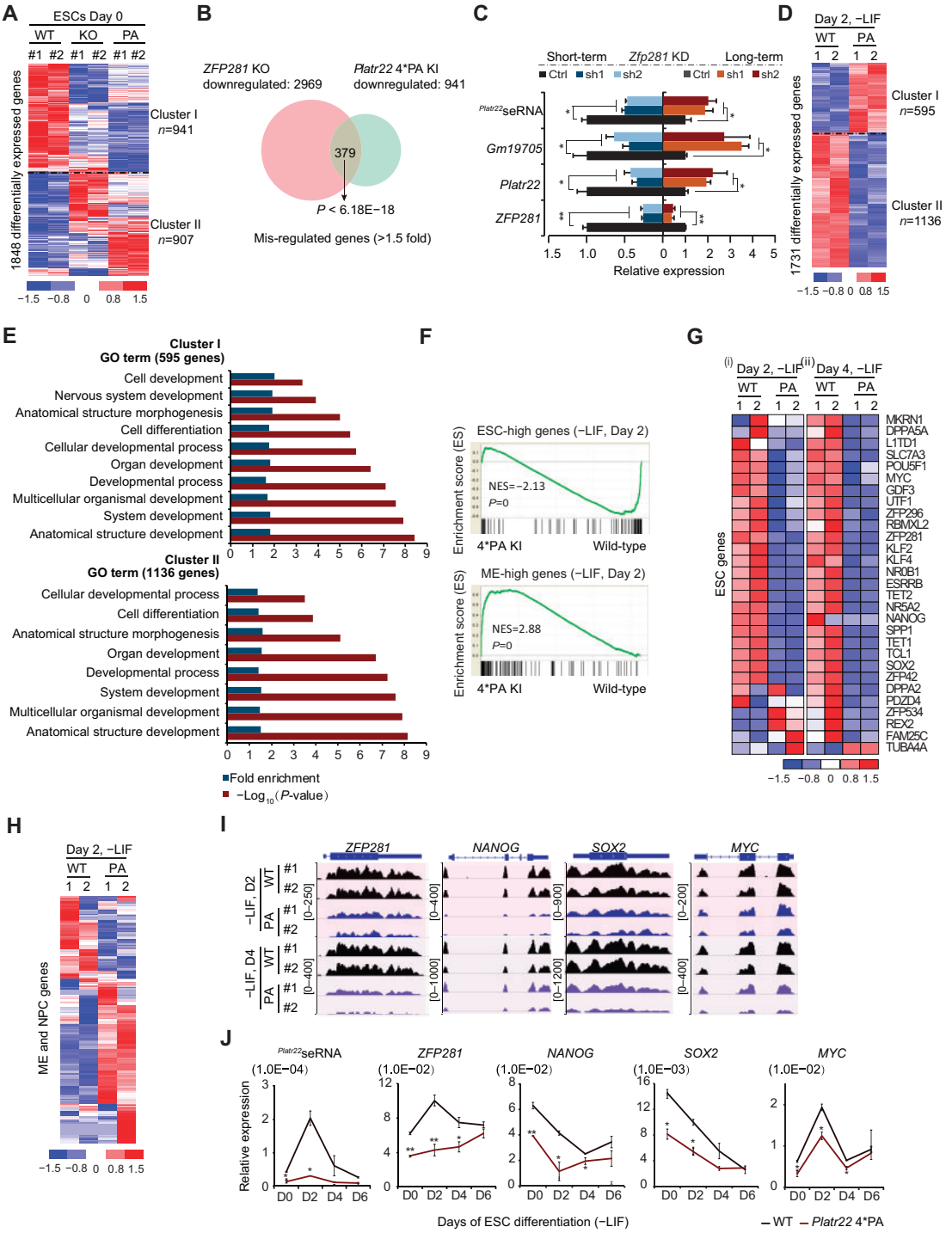

Figure 4 Inhibition of *Platr22* promotes differentiation of ESCs. (**A**) Raw normalized expression of 1848 genes that are differentially expressed in *Platr22* 4*PA KI and *Platr22* KO ESCs on Day 0. The scale represents the Z-score. (**B**) Venn diagram showing the overlapping genes that are affected by both *Platr22* 4*PA KI and *ZFP281* KO. (**C**) RT-qPCR analysis for short-term (48 h) and long-term (96 h) effects of *ZFP281* RNAi. Data are shown as mean ± SD ($n = 4$, including two technical repeats for two independent biological replicates). $^*P < 0.05$, $^{**}P < 0.01$. (**D**) Raw normalized expression of 1731 genes that are differentially expressed in *Platr22* 4*PA KI mESCs on Day 2 after LIF withdrawal. (**E**) GO analysis of genes that are dysregulated in *Platr22* 4*PA KI cells on Day 2 after LIF withdrawal. (**F**) *Platr22* 4*PA KI ESCs show global downregulation of ESC-high genes and upregulation of ME-high genes by GSEA on Day 2 after LIF withdrawal. NES and nominal *P*-value are shown. (**G**) Heatmap of the expression of representative ESC-related genes in *Platr22* 4*PA KI ESCs on Day 2 (i) and Day 4 (ii) of ESC differentiation. (**H**) Heatmap of the expression of representative ME- and NPC-related genes in *Platr22* 4*PA KI ESCs on Day 2 of ESC differentiation. (**I**) RNA-seq tracks of *ZFP281*, *NANOG*, *SOX2*, and *MYC* in WT and *Platr22* KO ESCs on Day 2 or Day 4 of differentiation induced by LIF withdrawal. (**J**) RT-qPCR time-course analysis of marker genes in WT, *Platr22* KO, and Platr22 4*PA KI ESCs during differentiation.

Platr22 regulates differentiation of mESCs

During leukemia inhibitory factor (LIF) withdrawal-induced mESC differentiation, the expression of *Platr22*, *ZFP281*, and ^{Platr22}seRNA was first upregulated to reach a peak on Day 2 and then downregulated during prolonged differentiation (Supplementary Figure S4D). To examine whether *Platr22* also plays a role during mESC differentiation, we performed RNA-seq analysis of *Platr22* 4*PA KI cells after withdrawal of LIF for 2 or 4 days (Supplementary Table S3). Depletion of *Platr22* upregulated the expression of 595 genes and downregulated 1136 genes on Day 2 of mESC differentiation (fold change >1.5, and $P<0.05$; Figure 4D). These dysregulated genes are significantly enriched in developmental process-related terms (Figure 4E). Similar expression changes were also observed on Day 4 of mESC differentiation (Supplementary Figure S4E and F). We further performed gene set enrichment analysis (GSEA) to explore the functional implications of these altered gene expression profiles. Compared to WT control mESCs, *Platr22* 4*PA KI mESCs exhibit a substantial downregulation of ESC-enriched genes [ESC-high, normalized enrichment score (NES) $= -2.13$, $P=0$] and neuronal progenitor cell-enriched genes (NPC-high, NES $= -1.42$, $P=0.02$), while mesendoderm-enriched genes were upregulated (ME-high, NES $= 2.88$, $P=0$) on Day 2 of mESC differentiation (Figure 4F–H; Supplementary Figure S4G, H and Table S4). Notably, representative pluripotency genes such as *ZFP281*, *NANOG*, *SOX2*, and *MYC* are substantially downregulated, which was further confirmed by RT-qPCR (Figure 4I and J). These results suggest that *Platr22* is required for proper differentiation of mESCs, and depletion of *Platr22* transcripts promotes mESC differentiation, especially to mesoderm and endoderm lineages.

Next, we sought to investigate the effect of continuously overexpressing *Platr22* transcripts during mESC differentiation. We used TetO KI mESCs to alter the expression of *Platr22* transcripts during differentiation. As *Platr22* transcription is upregulated during the first 2 days of differentiation (Supplementary Figure S4D), we chose to add DOX at Day 3 after LIF withdrawal (Figure 5A). We harvested RNA at 8, 24, 48, and 72 h after DOX induction. The expression of *Platr22* RNA was upregulated by 4- to 6-fold upon DOX treatment, and the expression of ^{Platr22}seRNA was also elevated by 1.5- to 6-fold (Figure 5B). Interestingly, the expression of *ZFP281* was upregulated by ~2-fold at 8 h of DOX treatment, and then dropped to levels similar to the control at later time points (Figure 5B). We then performed RNA-seq to characterize transcriptome-wide RNA expression changes in the presence of DOX-induced *Platr22* transcription (Supplementary Table S5). Compared to the control (no DOX treatment), 1590 differentially expressed genes were identified (fold change >1.5, $P<0.05$), which could be divided into three clusters (Supplementary Figure S5A): (i) cluster I genes are upregulated at 8 h and downregulated at 24 h, and then slightly upregulated at 72 h; (ii) cluster II genes are downregulated at both 8 and 24 h and upregulated at 72 h; and (iii) cluster III genes are downregulated at 8 h, and significantly upregulated at 24 and 72 h (Supplementary Figure S5A). GO analysis of these gene clusters revealed that clusters I and III are significantly enriched in GO terms associated with developmental processes and cell differentiation, while cluster II is enriched for GO terms linked to metabolic processes (Supplementary Figure S5B). These GO terms are consistent with previously reported processes related to *ZFP281* (Fidalgo et al., 2012).

GSEA suggested a global upregulation of ESC-high genes upon persistent induction of *Platr22* transcription, while the expression of ME-high genes was first downregulated at 8 h of *Platr22* induction and then upregulated at later time points (Figure 5C and D; Supplementary Table S4). Representative ESC-high genes like *ZFP42*, *TCL1*, and *Pou5f1*, as well as mesendodermal genes like *EOMES*, *T*, *GSC*, *GATA6*, and *SNAIL1*, were dysregulated in *Platr22*-overexpressing cells (Figure 5E). This result indicates that a suitable level of *Platr22* transcripts is required for proper mESC differentiation. Taken together, our *Platr22* depletion and overexpression results suggest that *Platr22* regulates the activity of ^{Platr22}SE and contributes to the pluripotency maintenance and proper differentiation of mESCs.

Platr22 interacts with DDX5 and hnRNP-L to modulate ^{Platr22}SE activity and ZFP281 expression

To determine the mechanism by which *Platr22* modulates the activity of ^{Platr22}SE, we sought to identify the *in vitro* and *in vivo* interactome of *Platr22* transcripts through three different approaches. Briefly, we performed *in vitro* RNA pull-down assays by incubating nuclear extracts from mESCs with *in vitro*-transcribed biotinylated or strepto-tagged *Platr22* RNA (Supplementary Figure S6A). We also performed comprehensive identification of RNA-binding proteins (RBPs) by mass spectrometry (ChIRP–MS) to capture endogenous *Platr22* RNA and its interactome directly through antisense biotinylated probes (Chu et al., 2015). We then focused on four candidate proteins (DDX5, DDX17, NCL, and hnRNP-L) identified by all three approaches (Figure 6A; Supplementary Figure S6B and Table S6). Using RNA pull-down coupled with western blotting, we showed that DDX5 and hnRNP-L, but not the other two, specifically interact with *Platr22* RNA *in vitro* (Figure 6B; Supplementary Figure S6C). To further explore whether *Platr22* transcripts interact with DDX5 and hnRNP-L *in vivo*, we performed RNA immunoprecipitation (RIP) by using antibodies against DDX5 and hnRNP-L. Both of these antibodies captured a substantially larger amount of *Platr22* RNA than the IgG control (Figure 6C and D; Supplementary Figure S6D). Thus, by using complementary approaches, we confirmed that *Platr22* transcripts interact with DDX5 and hnRNP-L both *in vitro* and *in vivo*.

We then performed chromatin immunoprecipitation (ChIP) using antibodies against hnRNP-L and DDX5 and analyzed their binding at the ^{Platr22}SE region through qPCR. Both hnRNP-L and DDX5 were highly enriched at the ^{Platr22}SE region (Figure 6C and E). Notably, the binding of DDX5 to ^{Platr22}SE was

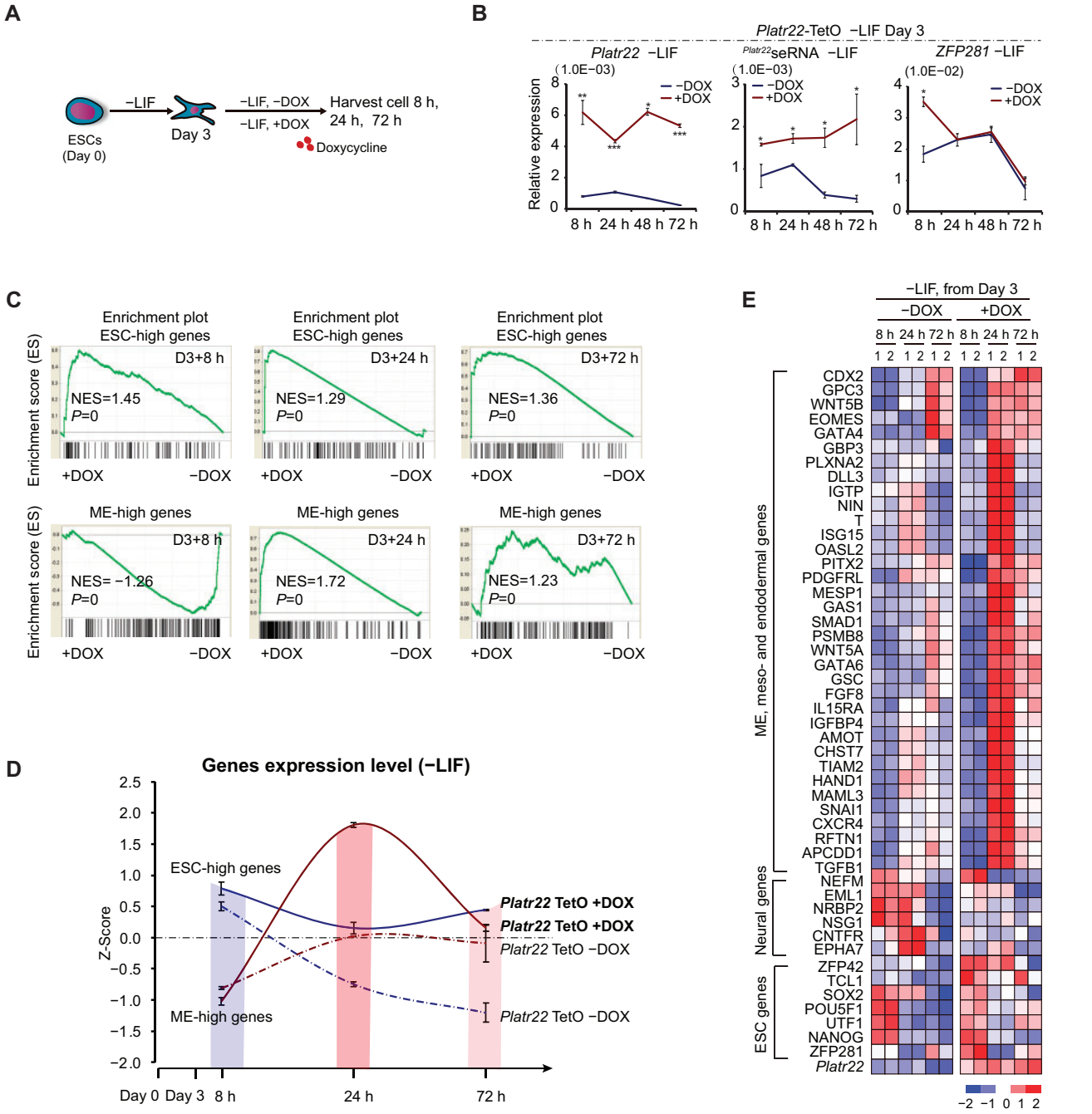

Figure 5 High-level transcription of *Platr22* promotes ESC differentiation. (**A**) The procedure for differentiation of ESCs with DOX treatment is shown. LIF was withdrawn on Day 0 and cells were induced with DOX from Day 3. Cells were harvested at different time points after the onset of DOX treatment for analysis. (**B**) RT-qPCR time-course analysis of *Platr22* RNA, ^{Platr22}seRNA, and *ZFP281* RNA expression in cells from **A**. Times (8, 24, 48, and 72 h) are following the onset of DOX treatment from Day 3 of ESC differentiation. (**C**) GSEA shows global upregulation of ESC-high genes in *Platr22*-tetO KI ESCs upon DOX treatment from Day 3 of differentiation (upper). ME-high genes show global downregulation at 8 h and upregulation at 24 and 72 h of DOX treatment. NES and nominal *P*-value are shown. (**D**) The expression patterns of ESC-high and ME-high genes are shown in *Platr22*-tetO KI cells at 8, 24, and 72 h with or without DOX treatment from Day 3 of ESC differentiation. (**E**) Heatmap of the expression of representative genes at 8, 24, and 72 h with or without DOX treatment from Day 3 of ESC differentiation.

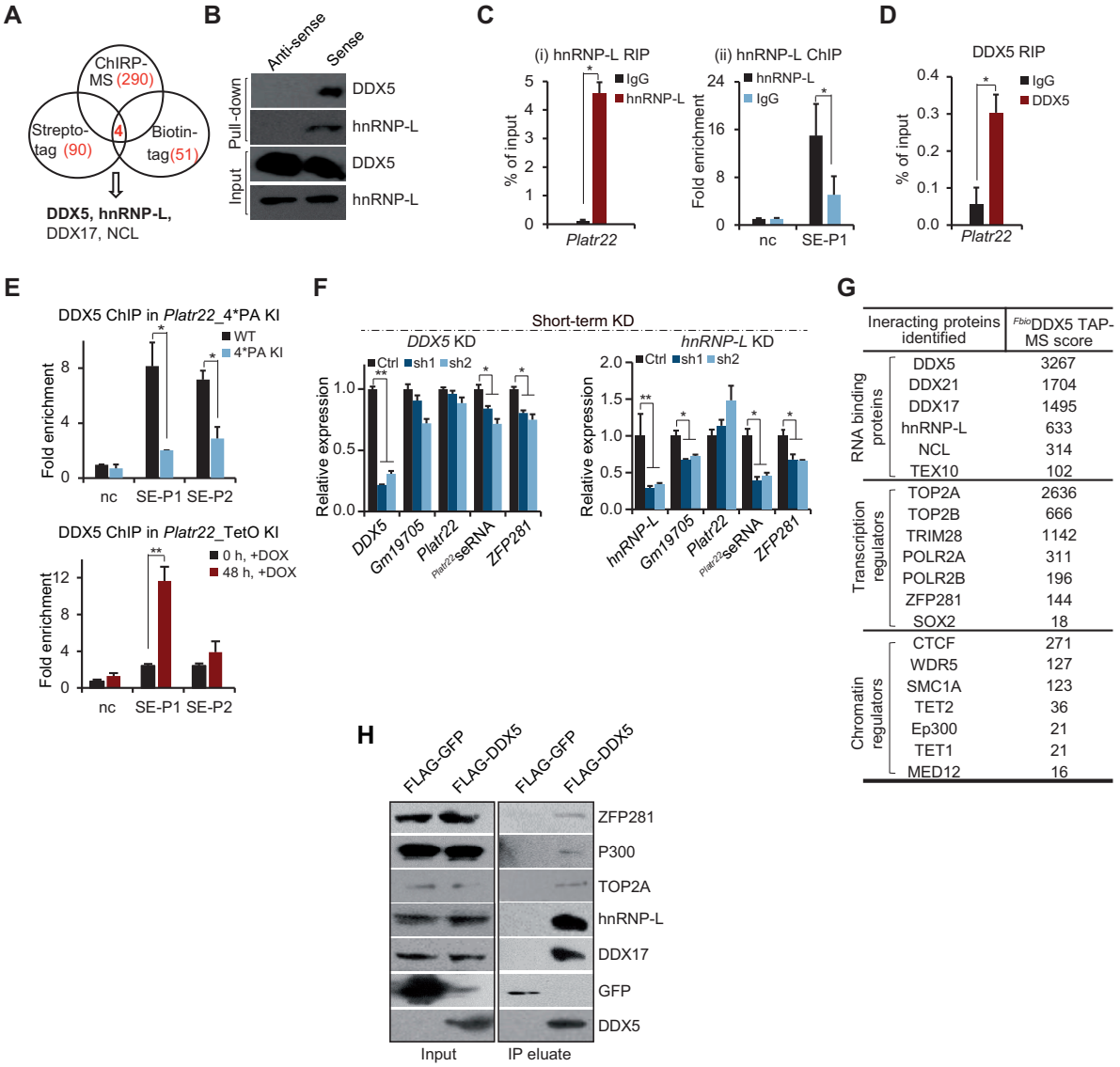

	Ineracting proteins identified	FbioDDX5 TAP-MS score
RNA binding proteins	DDX5	3267
	DDX21	1704
	DDX17	1495
	hnRNP-L	633
	NCL	314
	TEX10	102
Transcription regulators	TOP2A	2636
	TOP2B	666
	TRIM28	1142
	POLR2A	311
	POLR2B	196
	ZFP281	144
	SOX2	18
Chromatin regulators	CTCF	271
	WDR5	127
	SMC1A	123
	TET2	36
	Ep300	21
	TET1	21
	MED12	16

Figure 6 *Platr22* modulates its nearby transcription hub by mediating recruitment of DDX5 and hnRNP-L to the ^{Paltr22}SE region. (**A**) Overlap analysis of the results from ChIRP–MS, strepto-tag pull-down, and biotin-tag pull-down. (**B**) RNA pull-down assays of *Platr22* RNA-associated proteins with antibodies to DDX5 and hnRNP-L. *Platr22*-antisense transcripts served as the control. (**C**) (i) RIP–qPCR of hnRNP-L. The y-axis shows the percentages of input. (ii) ChIP–qPCR of hnRNP-L. The y-axis shows fold enrichment relative to the 'nc' (CSa). (**D**) RIP–qPCR of DDX5. The y-axis shows percentages of input. (**E**) ChIP–qPCR of DDX5 in *Platr22* 4*PA KI and *Platr22*-TetO KI cell lines. The y-axis shows fold enrichment relative to the 'nc' (CSa). (**F**) RT-qPCR analysis for the short-term (48 h) effects of *DDX5* or *hnRNP-L* KD. The y-axis shows expression normalized to *GAPDH*. (**G**) Summary of the interacting proteins identified by ^{Fbio}DDX5 TAP. (**H**) Co-IP of FLAG-DDX5 with antibodies to ZFP281, p300, TOP2A, hnRNP-L, and DDX17. All data are shown as mean± SD ($n = 4$, including two biological replicates and two technical replicates). *$P < 0.05$, **$P < 0.01$.

substantially decreased in GFP-4*PA KI mESCs and increased in TetO KI cells upon DOX induction for 48 h (Figure 6E). This result suggests the binding intensity of DDX5 to the SE region is regulated by *Platr22*.

Next, to further explore whether DDX5 and hnRNP-L are involved in the regulation of ^{Platr22}SE by *Platr22*, we inhibited the expression of these two proteins through shRNA KD. Depletion of *DDX5* or *hnRNP-L* substantially impaired the expression of ^{Platr22}seRNA and *ZFP281*, but not *Platr22* (Figure 6F; Supplementary Figure S6E). This suggests that *Platr22* RNA modulates the activity of ^{Platr22}SE and expression of *ZFP281* mainly through its interacting proteins DDX5 and hnRNP-L.

Finally, to further investigate how the *Platr22*–DDX5/hnRNP-L complex modulates the activity of ^{Platr22}SE, we constructed a

mESC line stably expressing FLAG-biotin-tagged DDX5 (herein referred to as ^{Fbio}DDX5 mESCs). Consistent with the DDX5 ChIP results presented above, biotin-streptavidin-mediated ChIP (bioChIP) analysis of ^{Fbio}DDX5 mESCs also captured large amounts of ^{Platr22}SE genomic DNA (Supplementary Figure S6F). We then performed FLAG- and biotin-mediated tandem affinity purification followed by mass spectrometry (TAP–MS) with nuclear extracts from ^{Fbio}DDX5 mESCs to identify the interactome of DDX5 (Supplementary Figure S6G). Interestingly, besides RBPs including hnRNP-L and DDX5, TAP–MS also identified regulators of transcription and chromatin structure such as *ZFP281*, p300, and TOP2A (Figure 6G). We further confirmed the interaction between DDX5 and these proteins by performing co-immunoprecipitation (co-IP) with an anti-FLAG antibody in ^{Fbio}DDX5 mESCs or control mESCs expressing FLAG-tagged GFP (Figure 6H). The interactions between DDX5 and p300 and other transcription regulators link *Platr22* transcripts and the binding proteins directly to modulate the activity of ^{Platr22}SE and the expression of *ZFP281*.

Discussion

Dynamic and intricate regulation of gene expression is critical for cell fate determination and development. Previous studies have identified large numbers of *trans* factors, including master transcription factors, epigenetic regulators, etc., that regulate the activity of SEs (Brown et al., 2014; Hah et al., 2015; Sengupta et al., 2015). The role, if any, of *cis*-regulatory noncoding sequences, especially lncRNAs, in regulating the activity of SEs remain elusive. In this study, we revealed an unanticipated juxtaposition between lncRNA genes and SEs and a general regulatory role of SE-lncRNA genes in modulating SE activity. We speculate that the association between SEs and lncRNA genes represents an additional layer of regulation for SE activity, which participates in the regulation of the formation, activity, and vulnerability to perturbation of SEs.

Previously, it has been demonstrated that most lncRNA genes preferentially modulate nearby transcription and participate in biological processes, which are similar to their nearby protein-coding genes (Orom et al., 2010; Luo et al., 2016; Hou et al., 2017; Werner et al., 2017). Our analysis suggests that lncRNA genes are more highly enriched than protein-coding genes in the vicinity of SEs, which is also supported by a previous study in T helper cells (Witte et al., 2015). The association between lncRNA genes and SEs suggests a biologically functional correlation between the two. For example, *NeST*, *lincR-Epas1-3'-AS*, and *lincR-Gata3-3'* are defined as SE-lncRNA genes, which play key roles in microbial susceptibility and development of T cells (Gomez et al., 2013; Hu et al., 2013). Cardiac mesoderm enhancer-associated ncRNA (*CARMEN*, *AK087736*), which is derived from a human cardiac SE, plays a key role in cardiac differentiation (Hnisz et al., 2013). *WISP2* SE-associated lncRNA (*Wisper*) may represent an attractive therapeutic target to prevent cardiac fibrosis and pathological remodeling (Micheletti et al., 2017). These individual case studies strongly support the notion that SE-lncRNA genes participate in the same biological process as the engaged SE.

Several lines of evidence suggest that SE-lncRNA genes mainly function through regulating the activity of nearby SEs. First, SE-lncRNA pairs exhibit significantly higher conservation and correlation of genomic position than TE-lncRNA and SE-coding pairs. Second, when selected lncRNAs were knocked down, ~90% of them dysregulated the activity of their nearby SEs. Specifically, loss- and gain-of-function analysis of *Platr22* transcripts led to the dysregulation of ^{Platr22}SE. Third, *Platr22* transcripts bind to the ^{Platr22}SE region and orchestrate histone H3K27ac on the ^{Platr22}SE region, thus providing mechanistic evidence that lncRNAs mediate *cis*-regulation of nearby SE activity. Thus, lncRNA represents an additional component for manipulating nearby SE activity, together with previously reported transcription factors (Hnisz et al., 2013; Whyte et al., 2013; Brown et al., 2014; Adam et al., 2015; Ding et al., 2015; Shin et al., 2016).

One intriguing question is that why lncRNAs preferentially lie next to SEs. We believe that two possibilities may contribute to this observation. On the one hand, compared to protein-coding mRNAs, eRNAs and lncRNAs share many similar features, including inefficient or no splicing, chromatin association, low-level expression, and short half-lives (Clark et al., 2012; Li et al., 2016; Yin et al., 2020). Moreover, more and more pieces of evidence suggest that lncRNAs may originate from eRNAs and promoter-associated unstable transcripts (PROMPTs) (Wu and Sharp, 2013; Alvarez-Dominguez et al., 2017; Espinosa, 2017). These feature similarities and origination connection blur the distinction between lncRNAs and eRNAs. On the other hand, compared to eRNAs, lncRNAs have been better characterized and annotated (Derrien et al., 2012). The first distinction is that lncRNAs were broadly defined based on the presence of H3K4me3, a canonical histone mark of active gene promoters (Guttman et al., 2009), while eRNAs can usually be produced from enhancers with H3K4me1 histone modification instead of H3K4me3. In addition, compared to eRNAs, lncRNAs tend to be longer, more stable, better processed, and unidirectionally transcribed (Li et al., 2016). RNAs transcribed from enhancer regions have been reported to stimulate CBP/p300's histone acetyltransferase activity and play a vital role in proper enhancer activity (Li et al., 2016; Bose et al., 2017). We proposed that the relatively abundant and stable lncRNAs may show a stronger ability to promote the enhancer activity than the unstable eRNAs with lower expression levels. In support of this notion, we have shown that the depletion of SE-lncRNAs compromised the activity of their nearby SEs (Figures 1E and 2B). The strong enhancer activity of SE may also have a greater opportunity to contribute to the high expression of its associated lncRNA, and thus form a positive feedback loop.

Intriguingly, unlike the short-term *Platr22* overexpression, the long-term *Platr22* overexpression decreased the expression of seRNA and *ZFP281* (Figure 3H). A potential explanation for this discrepancy is that compensatory regulation may be activated during persistently overexpressing *Platr22*. This

regulation mainly through modulating the expression of *ZFP281*. ZFP281 was reported to function as both transcription activator and repressor—on the one hand, it physically interacts with OCT4, SOX2, and NANOG and binds to the promoter of *NANOG* to activate *NANOG* expression; on the other hand, it recruits NuRD repressor complex onto *NANOG* locus to mediate *NANOG* autorepression (Wang et al., 2008; Fidalgo et al., 2011, 2012). This autonomous regulation safeguards proper *NANOG* expression for ES pluripotency maintenance and differentiation. Prolonged *Platr22* overexpression might trigger this autonomous regulation and feedback on the downregulation of seRNA and *ZFP281*.

In addition, it has been reported that the seRNA–hnRNP-L partnership can regulate the expression of its target gene *Mb* (Zhao et al., 2019). The seRNA-1 controls the precise dose of hnRNP-L at its target gene, low-level binding of hnRNP-L at the *Mb* promoter facilitates *Mb* gene expression, while high dosage of hnRNP-L at the promote inhibits expression (Zhao et al., 2019). Chromatin-bound seRNA-1 facilitates hnRNP-L binding at the *Mb* promoter. When seRNA leaves the chromatin, it brings away hnRNP-L, thereby reducing the dose of hnRNP-L at the promoter (Zhao et al., 2019). We propose that eRNA–DDX5, eRNA–hnRNP-L, and other co-factors have a similar mechanism contributing to controlling the precise dose of the SE activity, which participates in the regulation of the formation, activity, and vulnerability to perturbation of SEs.

SEs are reported to be occupied by a high density of interacting factors and are exceptionally vulnerable to perturbation, which is important for SE formation and function (Hnisz et al., 2017). In this study, we established that *Platr22* transcripts regulate ^{Platr22}SE activity by interacting with DDX5, hnRNP-L, and other co-factors. DDX5 was reported to interact with the noncoding RNA *SRA* as coactivators in the Notch signaling pathway (Jung et al., 2013). Notably, there is evidence that DDX5 functions as a p53-independent target of the ARF tumor suppressor and is involved in ribosome biogenesis and cell proliferation (Jalal et al., 2007; Saporita et al., 2011). However, *DDX5* KO had no effect on the expression of pluripotency genes *POU5F1*, *NANOG*, *SOX2*, and *UTF1* (Li et al., 2017a). Our result also suggests that long-term depletion of *DDX5* has a subtle effect on the expression of *Platr22*, ^{Platr22}seRNA, and *ZFP281* (Supplementary Figure S6E). A potential explanation for this discrepancy is that compensatory regulation may be activated during long-term or complete depletion of *DDX5*, which rescued the dysregulation of pluripotency genes. *hnRNP-L* is well-known for its function in regulating alternative splicing (Hung et al., 2008; Han et al., 2010; Fei et al., 2017), and it was also reported to interact with the lncRNA *THRIL* to regulate *TNF* expression (Li et al., 2014b). Moreover, hnRNP-L was also reported to interact with seRNAs by binding to the CAAA motif, thus contributing to target gene activation (Zhao et al., 2019). These studies, together with our findings, imply that lncRNA–RBP complexes might be a general regulatory apparatus in regulating the activity of SE.

Interestingly, the DDX5 interactome includes several classes of proteins, such as RBPs, transcription regulators, and chromatin regulators. The interaction between DDX5 and p300 is consistent with previous reports (Rossow and Janknecht, 2003; Shin and Janknecht, 2007). Besides, another *Platr22* RNA-interacting protein, DDX17, was reported to cooperate with p300/CBP and P/CAF to directly regulate gene transcription (Jalal et al., 2007; Shin and Janknecht, 2007), and the RNA helicase DDX21 was reported to coordinate transcription and control ribosome biogenesis in human cells (Calo et al., 2015). In addition, another interacting RBP, TEX10, was reported to be required for pluripotency maintenance and efficient reprogramming through regulating the epigenetic status and activity of SEs (Ding et al., 2015). Thus, based on the interactome of *Platr22* and DDX5, it is reasonable to speculate that *Platr22*, together with these RBPs and transcription regulators, assemble into a transcription hub to modulate ^{Platr22}SE activity and *ZFP281* expression. By analyzing previously reported ZFP281 ChIP-seq data, we found that ZFP281 binds to the promoters of pluripotent regulators such as *NANOG*, *POU5F1*, *SOX2*, and *MYC*, as well as the promoters of itself and *Platr22* (Supplementary Figure S6H), suggesting that *ZFP281* might directly regulate the expression of these pluripotent genes (Fidalgo et al., 2011, 2012; Huang et al., 2017). It also implies that ZFP281, together with *Platr22* and pluripotency regulators, may form an autonomous regulatory loop, which safeguards the proper expression of pluripotency genes, and thus contribute to the regulation of mESC pluripotency (Figure 7).

We identified six lncRNA genes that promoted the activity of their nearby SEs and two lncRNA genes that negatively

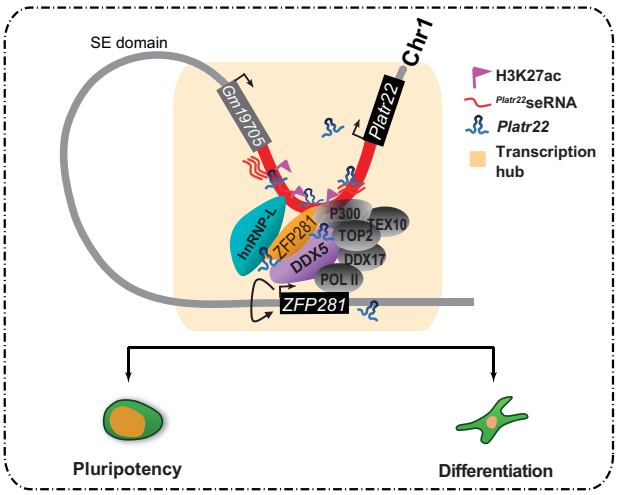

Figure 7 Model for how *Platr22* regulates SE activity and stem cell pluripotency. *Platr22* transcripts coat the chromatin of the nearby SE region and interact with DDX5 and hnRNP-L. DDX5 further recruits p300 and other factors related to active transcription, which assemble into a transcription hub, thus promoting an open and active epigenetic chromatin state. The role of *Platr22* RNA is to modulate the activity of ^{Platr22}SE and the expression of *ZFP281*, which is required for orchestrated lineage differentiation of ESCs.

regulated their nearby SEs (Figure 1E). This subset of negative regulatory lncRNA genes may function through RNA-mediated local recruitment of transcriptional repressors or chromatin-remodeling factors that repress transcription factor binding or through a transcription competition mechanism as previously reported (Rinn et al., 2007; Latos et al., 2012; Klattenhoff et al., 2013; Gil and Ulitsky, 2020). Nevertheless, our results raise the possibility that SE-lncRNA genes mediate transcription regulation and formation of nearby SEs, which may represent a common mechanism for orchestrating biological processes controlled by nearby SEs.

Several lines of evidence have revealed that SEs are more sensitive than TEs to perturbation of transcriptional co-factors (Hnisz et al., 2017; Khan et al., 2018; Sabari et al., 2018). Interestingly, studies have shown that multiple factors have the ability to involve or facilitate intermolecular interactions through a phase-separation mechanism (Boeynaems et al., 2018; Boija et al., 2018; Gurumurthy et al., 2019; Palikyras and Papantonis, 2019). Moreover, it was reported that a single enhancer can simultaneously activate multiple proximal genes in bursts, and the formation of SEs may facilitate phase separation for transcription control (Fukaya et al., 2016; Hnisz et al., 2017). The hub formed by *Platr22* RNA and its interacting proteins may modulate the activity of ^{Platr22}SE through a phase-separation mechanism. *Platr22* transcripts may be the key to this model, as perturbation of *Platr22* RNA levels severely impaired the formation and dissolution of this hub. Although the detailed mechanism needs to be further investigated, we believe that the linkage between lncRNAs and SEs will help us to better understand the mechanisms by which lncRNA genes function and the activity of SEs is regulated, as well as how they participate in gene expression regulation and cell fate determination.

Materials and methods

ESC culture and differentiation

WT (46C) and various KO and KI ESCs were cultured on gelatin-coated plates in standard ESC culture medium: Dulbecco's modified Eagle's medium (DMEM) supplemented with 15% heat-inactivated fetal bovine serum (Hyclone), 1% penicillin–streptomycin (Cellgro), 1% of nucleoside mix (100× stock, Millipore), 1% Glutamax (GIBCO), 1% MEM nonessential amino acids (Cellgro), 0.1 mM 2-mercaptoethanol, and 1000 U/ml recombinant LIF (Millipore). For differentiation time course with LIF withdrawal, cells were harvested at Day 0, Day 2, Day 4, and Day 6 of differentiation.

RNAi and ectopic overexpression

We randomly selected 10 SE-lncRNA pairs with fragments per kilobase of exon model per million mapped reads (FPKM) of chromatin-associated lncRNAs >1 in ESCs. Only nine lncRNAs were knocked down by at least one shRNA. RNAi was performed as described previously (Shen et al., 2008). We used lentivirus-mediated (pLKO vector) RNAi (Moffat et al., 2006). Lentivirus was packaged and generated in 293T cells and then infected ESCs, which were selected by puromycin for 72 h. Cells were harvested for RNA extraction and RT-qPCR analysis. For ectopic overexpression of *Platr22*, *Platr22* transcript was driven by the CAG promoter in PiggyBac and cotransfected with pBASE into ESCs, which were selected for 5 days by hygromycin before RNA extraction and RT-qPCR analysis.

CRISPR/Cas9-mediated KO and KI

CRISPR/Cas9 was performed as previously described and modified (Yin et al., 2015; Luo et al., 2016). Plasmids expressing Cas9 ('pST1374-N-NLS-flag-linker-Cas9', Addgene ID 44758) and sgRNAs ('pGL3-U6-sgRNA') were cotransfected into ESCs by lipofectamine 2000 (Shen et al., 2008, 2013). For KO, Cas9 and two sgRNAs targeting the genomic deletion region were cotransfected into ESCs. For KI, Cas9 and one sgRNA targeting the site of insertion and one sgRNA targeting the vector for linearization, which mediated non-homologous recombination and precise insertion into targeting sites, were cotransfected into ESCs. Targeting vectors contain a GFP-4xpolyA, TetO promoter sequence, and a hygromycin selection cassette (PGK-hygro). The PGK-hygro cassettes were excised by CRE recombinase and single clones were picked.

CRISPR/Cas9-mediated activation, interference, and RNA tethering

CRISPR-on was performed as previously described (Konermann et al., 2015). Plasmids expressing dCas9-VP64 (Addgene #61425), MS2-P65-HSF1 (Addgene #61426), and sgRNA (fused with MS2, containing a puromycin cassette) were cotransfected into ESCs by lipofectamine 2000 (Life Technologies). Cells were harvested after puromycin and blasticidin selection for RNA isolation and RT-qPCR analysis.

CRISPRi was performed as previously described and modified (Larson et al., 2013). Plasmids expressing pHR-SFFV-dCas9-BFP-KRAB (Addgene #46911) and gRNA (containing a puromycin cassette) were cotransfected into ESCs. sgRNAs were designed to target the *Platr22* nearby SE region and the TSS of *Platr22*. Cells were harvested for RT-qPCR analysis after 2 days of selection by puromycin.

RNA tethering was performed as previously described (Shechner et al., 2015; Luo et al., 2016). The *Platr22*-sense RNA (*Platr22*-S), antisense RNA (*Platr22*-AS), and GFP RNA were fused to sgRNAs targeting the *Platr22* nearby SE region. These plasmids were cotransfected with dCas9 into ESCs, respectively. Cells were harvested for RT-qPCR analysis after 2 days.

Subcellular fractionation assay

Subcellular fractionation was performed as previously described and modified (Bhatt et al., 2012; Yin et al., 2015). One

10-cm plate of ESCs were harvested and washed with ice-cold phosphate-buffered saline (PBS). The cell pellet was resuspended in 200 μl cold cytoplasmic lysis buffer (0.15% NP-40, 10 mM Tris, pH7.5, and 150 mM NaCl) on ice for 5 min, and then the lysate was transferred onto 500 μl ice-cold sucrose buffer (10 mM Tris, pH 7.5, 150 mM NaCl, and 24% sucrose). The supernatant was collected as the cytoplasmic fraction after spinning at 13000 rpm for 3 min.

The nuclear pellet was gently resuspended into cold glycerol buffer (20 mM Tris, pH 7.9, 75 mM NaCl, 0.5 mM EDTA, 50% glycerol, and 0.85 mM DTT). An additional cold nuclei lysis buffer (20 mM HEPES, pH 7.6, 7.5 mM $MgCl_2$, 0.2 mM EDTA, 0.3 M NaCl, 1 M urea, 1% NP-40, and 1 mM DTT) was added to the samples, followed by a pulsed vortex and incubation on ice for 1 min. Samples were then spin for 2 min at 14000 rpm and 4°C. The supernatant represented the nucleoplasm fraction.

Cytoplasmic and nucleoplasm RNA was purified by using TRIzol reagent (Life Technology). Chromatin pellet was extracted by TRIzol reagent upon heating for 10 min at 65°C.

ChIRP

ChIRP was performed as previously described with modifications (Yin et al., 2015; Luo et al., 2016). The 59-nt DNA biotinylated probes (Sangon Biotech) and more stringent wash conditions were employed. The probes were biotinylated with Bio-N6-ddATP (ENZO, ENZ-42809) by using terminal transferase (NEB, M0315S). About 5×10^7–1×10^8 ESCs were harvested and washed twice by ice-cold PBS. Crosslinking was performed as follows steps: 300 mJ UV twice, 0.8% formaldehyde (FMA) for 10 min at room temperature, 2 mM DSP (succinimidyl propionate) for 30 min, and 3.7% FMA for 10 min at room temperature. Cells were washed three times by using ice-cold PBS. Crosslinked cells were resuspended in nuclei lysis buffer (50 mM Tris-Cl, pH7.5, 10 mM EDTA, and 1% SDS) with treatment of protease inhibitor cocktail, PMSF, and RNaseOut. Sonication, hybridization, washing, and elution steps were performed as previously described (Yin et al., 2015). ChIRP samples were subjected to DNA-seq on a HiSeq 2500. Fold enrichment of chromatin association of *Platr22* was calculated by normalizing ChIRP signals to *Platr22* KO cells to minimize nonspecific targeting of ChIRP probes to chromatin DNA. For ChIRP DNA-seq data analysis, raw reads were mapped to the mouse genome (mm9) by using Bowtie v.1.0.0 (Langmead et al., 2009). Positive peaks were identified with the MACS program by comparing WT to *Platr22*-KO samples with a *P*-value cutoff of 1×10^{-5} (Zhang et al., 2008). The sequences of probe and primer are listed in Supplementary Table S1.

ChIP and RIP

ChIP was performed as previously described (Shen et al., 2008) with antibodies for H3K27ac (Abcam, ab4729) and DDX5 (Abcam, ab128928). Fold enrichment was normalized to an unrelated genomic region ('nc', primer CSa). RIP experiment was performed as described (Yang et al., 2014). RT-qPCR results are normalized to *GAPDH*.

RNA FISH

To detect *Platr22*, RNA FISH was performed as previously described (Xiang et al., 2014). *Platr22*-antisense probes were transcribed *in vitro* and labeled with digoxigenin. *Platr22*-sense probes were used as the control. WT ESCs and *Platr22* KO cells were cultured on cover glasses. Cells were fixed in 3.6% freshly prepared paraformaldehyde (PFA) with 10% acetic acid in PBS, incubated for 15 min at room temperature, washed three times with PBS at room temperature, permeabilized with 0.3% Triton X-100, and precipitated in 70% ethanol at 4°C for at least 1 h. After precipitation, cells were washed three times with washing buffer (2× SSC containing 10% formamide) and incubated with 50 μl of hybridization buffer (2× SSC with 100 mg/ml dextran sulfate and 10% formamide) containing probes at a dark humidified chamber for overnight. Then, the cells were washed twice and incubated with 1:500 diluted sheep anti-digoxigenin (Sigma) at 37°C for 1 h. The nuclei were stained with DAPI in PBS. Images were taken with a Zeiss LSM 780 microscope.

RNA pull-down and MS

RNA pull-down was performed as previously described and modified (Klattenhoff et al., 2013). Biotinylated *Platr22* RNAs were transcribed *in vitro* by T7 RNA polymerase (Ambion, AM1354). Then 2 μg of biotinylated RNA were heated for 10 min at 65°C and cooled down to room temperature in RNA structure buffer (10 mM Tris, pH 7, 0.1 M KCl, and 10 mM MgCl). About 5×10^7 cells were harvested and the nuclear pellets were extracted in 2 ml PBS, 2 ml nuclear isolation buffer (1.28 M sucrose, 40 mM Tris-HCl, pH 7.5, 20 mM MgCl2, and 4% Triton X-100), and 6 ml H_2O. After 20 min incubation on ice, the nuclei pellets were centrifuged at 2500 *g* for 15 min, resuspended in 1 ml RIP buffer (150 mM KCl, 25 mM Tris, pH 7.4, 0.5 mM DTT, 0.5% NP40, 1 mM PMSF, and protease inhibitor cocktail), homogenized by 20 strokes in a tight-fitting Dounce, and spun at 13000 rpm for 10 min at 4°C. Then the supernatant was pre-cleared with pre-equilibrated streptavidin M-280 dynabeads (Invitrogen) and 20 μg/ml yeast tRNA for 1 h at 4°C, incubated with *in vitro* transcripts at 4°C for overnight, followed by the addition of 40 μl pre-equilibrated M-280 dynabeads, incubation for 3 h at 4°C, and washing 4 × 5 min with RIP buffer. RNA/proteins complexes were eluted in 60 μl 2% SDS buffer at 95°C for 5 min, and the *Platr22*-binding proteins were identified by MS and analyzed by western blotting.

ChIRP–MS

ChIRP–MS was performed as previously described and modified (Chu et al., 2015). Twenty 15-cm dishes of cells were harvested and crosslinked in 3% formaldehyde for 30 min at room

temperature, and ChIRP was performed. For protein elution, beads were heated at 95°C for 5 min in SDS sample buffer and the elution was transferred to a fresh tube. The beads were eluted again and the elution was pooled together. Final protein complexes were run in 4%–12% bis-tris NuPAGE gels (Invitrogen) for MS. ChIRP probes are listed in Supplementary Table S7.

Strepto Tag RNA pull-down

Strepto Tag RNA pull-down assay was performed as previously described and modified (Windbichler and Schroeder, 2006). The *Platr22*-sense transcript was fused with the Strepto Tag (5′-GGAUCGCAUUUGGACUUCUGCCCGCAAGGGCACCACGGU CGGAUCC-3′) at its 5′ end and placed downstream of the T7 promoter in pJET vector. The *Platr22*-Strepto Tag RNA was transcribed *in vitro* by T7 RNA polymerase (Ambion, AM1354). *Platr22*-antisense transcript was performed as the control sample, and dihydrostreptomycin-coupled sepharose and column were prepared. RNA transcripts (50 pmol) were incubated for 5 min at 70°C and 15 min at 37°C and then hybridized to the column for 1 h. The column was washed twice and nuclear extracts were loaded to the column and incubated for 1 h. The proteins were eluted twice with 1 ml column buffer containing 10 μM streptomycin. The two eluents were pooled and concentrated by using 10 KD Microsep Advance Centrifugal Devices (PALL) at 3000 *g* for 40 min at 4°C. The supernatant was transferred to a fresh tube, heated 95°C in SDS sample buffer for 5 min, and then run in 4%–12% bis-tris NuPAGE gels (Invitrogen) for MS.

Identification of SE

SE was identified as previous (Hnisz et al., 2013; Whyte et al., 2013). In brief, we used H3K27ac ChIP-Seq data to create annotations of SEs. Mouse H3K27ac ChIP-Seq data were downloaded from ENCODE project (http://www.epigenomebrowser.org/ENCODE/) (The ENCODE Project Consortium, 2012). All ChIP-seq reads were aligned to the mouse genome assembly mm10 using Bowtie2 (version 2.2.2) (Langmead and Salzberg, 2012). The ChIP-seq peaks were called by MACS with default parameters (Zhang et al., 2008). ROSE was further used to separate SEs from TEs (https://github.com/stjude/ROSE) (Hnisz et al., 2013; Whyte et al., 2013). We used parameter '12.5 kb' as maximum distance between two regions that will be stitched together. In order to account for promoter biases, we also excluded regions contained within ±2500 bp from the TSS of protein-coding genes as potential enhancers. With these parameters, the SEs can be positioned in the upstream or even cover the promoter regions of coding genes. For human SEs, we got the annotation from Supplementary Table S2 from Hnisz et al. (2013).

Position analysis of enhancers and genes

SEs and TEs were identified as above. We used Gencode mV7 and V19 for mouse and human gene annotations, respectively (Frankish et al., 2019). To identify SE- or TE-associated genes, we used various sizes ranging over 0, 5, 10, . . ., 190, 195, and 200 kb as the cutoff. If the distance between enhancer and gene was less than the cutoff used, we termed this gene as 'enhancer-associated gene'. To evaluate the association level of genes and enhancers, we generated random genomic regions with equal size and number with annotated TE or SE and calculated the fold enrichment of the number of enhancer-associated genes to random genomic region-associated genes (Figure 1A).

RNA-seq and ChIP-seq analysis

Alignments of RNA-Seq data to mouse genome assembly mm10 were performed using Tophat v2.0.10 (Kim et al., 2013). FPKM were calculated by Cufflink 2.1.1 to represent expression levels of transcripts. Gencode v19 was used as the human gene annotation (Trapnell et al., 2012). The ChIP-seq data were analyzed as previously described.

Evolutionary age of lncRNA

Evolutionary age of lncRNA was calculated as previous (Luo et al., 2016), and lncRNA genes were dated on the vertebrate phylogenetic tree by following a previous strategy (Zhang et al., 2010). Sequences overlapping with protein-coding exons were filtered out to avoid bias caused by neighboring genes. Out of all vertebrate genome sequences targeted by the UCSC genome alignment pipeline, we chose a subset with relatively good assembly quality (as revealed by larger contig N50s) as the outgroup species. Branch numbers represent evolutionary age assignments. Smaller numbers mean older or greater evolutionary origins. Species names and corresponding genome assemblies are shown.

GO analysis

GO analysis was performed using DAVID bioinformatics tools (Huang da et al., 2009). *P*-value of Fisher's exact test was used to evaluate the enrichment of certain GO terms.

Gene set enrichment analysis

Gene set enrichment analysis was performed as previously (Luo et al., 2016). Gene sets including ESC-high, NPC-high, and ME-high were selected as previously described (Luo et al., 2016).

Supplementary material

Supplementary material is available at *Journal of Molecular Cell Biology* online.

Acknowledgements

We thank J. Wang, X. Fu, B. Zhou, and Shen laboratory members for insightful discussion and suggestions.

Funding

Grant support is from the National Basic Research Program of China (2017YFA0504204 and 2018YFA0107604), the National Natural Science Foundation of China (31630095 and 31925015), and the Center for Life Science at Tsinghua University.

Conflict of interest: none declared.

References

Adam, R.C., Yang, H., Rockowitz, S., et al. (2015). Pioneer factors govern super-enhancer dynamics in stem cell plasticity and lineage choice. Nature *521*, 366–370.

Alvarez-Dominguez, J.R., Zhang, X., and Hu, W. (2017). Widespread and dynamic translational control of red blood cell development. Blood *129*, 619–629.

Andersson, R., Gebhard, C., Miguel-Escalada, I., et al. (2014). An atlas of active enhancers across human cell types and tissues. Nature *507*, 455–461.

Bhatt, D.M., Pandya-Jones, A., Tong, A.J., et al. (2012). Transcript dynamics of proinflammatory genes revealed by sequence analysis of subcellular RNA fractions. Cell *150*, 279–290.

Boeynaems, S., Alberti, S., Fawzi, N.L., et al. (2018). Protein phase separation: a new phase in cell biology. Trends Cell Biol. *28*, 420–435.

Boija, A., Klein, I.A., Sabari, B.R., et al. (2018). Transcription factors activate genes through the phase-separation capacity of their activation domains. Cell *175*, 1842–1855.e16.

Bose, D.A., Donahue, G., Reinberg, D., et al. (2017). RNA binding to CBP stimulates histone acetylation and transcription. Cell *168*, 135–149.e22.

Brown, J.D., Lin, C.Y., Duan, Q., et al. (2014). NF-κB directs dynamic super enhancer formation in inflammation and atherogenesis. Mol. Cell *56*, 219–231.

Calo, E., Flynn, R.A., Martin, L., et al. (2015). RNA helicase DDX21 coordinates transcription and ribosomal RNA processing. Nature *518*, 249–253.

Chang, H.C., Huang, H.C., Juan, H.F., et al. (2019). Investigating the role of super-enhancer RNAs underlying embryonic stem cell differentiation. BMC Genomics *20*, 896.

Chappell, J., and Dalton, S. (2013). Roles for MYC in the establishment and maintenance of pluripotency. Cold Spring Harb. Perspect. Med. *3*, a014381.

Chu, C., Qu, K., Zhong, F.L., et al. (2011). Genomic maps of long noncoding RNA occupancy reveal principles of RNA–chromatin interactions. Mol. Cell *44*, 667–678.

Chu, C., Zhang, Q.C., Da Rocha, S.T., et al. (2015). Systematic discovery of Xist RNA binding proteins. Cell *161*, 404–416.

Clark, M.B., Johnston, R.L., Inostroza-Ponta, M., et al. (2012). Genome-wide analysis of long noncoding RNA stability. Genome Res. *22*, 885–898.

Derrien, T., Johnson, R., Bussotti, G., et al. (2012). The GENCODE v7 catalog of human long noncoding RNAs: analysis of their gene structure, evolution, and expression. Genome Res. *22*, 1775–1789.

Ding, J.J., Huang, X., Shao, N.Y., et al. (2015). Tex10 coordinates epigenetic control of super-enhancer activity in pluripotency and reprogramming. Cell Stem Cell *16*, 653–668.

Dixon, J.R., Selvaraj, S., Yue, F., et al. (2012). Topological domains in mammalian genomes identified by analysis of chromatin interactions. Nature *485*, 376–380.

Djebali, S., Davis, C.A., Merkel, A., et al. (2012). Landscape of transcription in human cells. Nature *489*, 101–108.

Espinosa, J.M. (2017). On the origin of lncRNAs: missing link found. Trends Genet. *33*, 660–662.

Fei, T., Chen, Y., Xiao, T., et al. (2017). Genome-wide CRISPR screen identifies HNRNPL as a prostate cancer dependency regulating RNA splicing. Proc. Natl Acad. Sci. USA *114*, E5207–E5215.

Fidalgo, M., Faiola, F., Pereira, C.F., et al. (2012). Zfp281 mediates Nanog autorepression through recruitment of the NuRD complex and inhibits somatic cell reprogramming. Proc. Natl Acad. Sci. USA *109*, 16202–16207.

Fidalgo, M., Huang, X., Guallar, D., et al. (2016). Zfp281 coordinates opposing functions of Tet1 and Tet2 in pluripotent states. Cell Stem Cell *19*, 355–369.

Fidalgo, M., Shekar, P.C., Ang, Y.S., et al. (2011). Zfp281 functions as a transcriptional repressor for pluripotency of mouse embryonic stem cells. Stem Cells *29*, 1705–1716.

Fong, H., Hohenstein, K.A., and Donovan, P.J. (2008). Regulation of self-renewal and pluripotency by Sox2 in human embryonic stem cells. Stem Cells *26*, 1931–1938.

Frankish, A., Diekhans, M., Ferreira, A.M., et al. (2019). GENCODE reference annotation for the human and mouse genomes. Nucleic Acids Res. *47*, D766–D773.

Fukaya, T., Lim, B., and Levine, M. (2016). Enhancer control of transcriptional bursting. Cell *166*, 358–368.

Gil, N., and Ulitsky, I. (2020). Regulation of gene expression by cis-acting long non-coding RNAs. Nat. Rev. Genet. *21*, 102–117.

Gomez, J.A., Wapinski, O.L., Yang, Y.W., et al. (2013). The NeST long ncRNA controls microbial susceptibility and epigenetic activation of the interferon-γ locus. Cell *152*, 743–754.

Gurumurthy, A., Shen, Y., Gunn, E.M., et al. (2019). Phase separation and transcription regulation: are super-enhancers and locus control regions primary sites of transcription complex assembly? Bioessays *41*, e1800164.

Guttman, M., Amit, I., Garber, M., et al. (2009). Chromatin signature reveals over a thousand highly conserved large non-coding RNAs in mammals. Nature *458*, 223–227.

Hah, N., Benner, C., Chong, L.W., et al. (2015). Inflammation-sensitive super enhancers form domains of coordinately regulated enhancer RNAs. Proc. Natl Acad. Sci. USA *112*, E297–E302.

Han, S.P., Tang, Y.H., and Smith, R. (2010). Functional diversity of the hnRNPs: past, present and perspectives. Biochem. J. *430*, 379–392.

Hnisz, D., Abraham, B.J., Lee, T.I., et al. (2013). Super-enhancers in the control of cell identity and disease. Cell *155*, 934–947.

Hnisz, D., Shrinivas, K., Young, R.A., et al. (2017). A phase separation model for transcriptional control. Cell *169*, 13–23.

Hou, J., Long, H., Zhou, C., et al. (2017). Long noncoding RNA Braveheart promotes cardiogenic differentiation of mesenchymal stem cells in vitro. Stem Cell Res. Ther. *8*, 4.

Hu, G., Tang, Q., Sharma, S., et al. (2013). Expression and regulation of intergenic long noncoding RNAs during T cell development and differentiation. Nat. Immunol. *14*, 1190–1198.

Huang da, W., Sherman, B.T., and Lempicki, R.A. (2009). Systematic and integrative analysis of large gene lists using DAVID bioinformatics resources. Nat. Protoc. *4*, 44–57.

Huang, X., Balmer, S., Yang, F., et al. (2017). Zfp281 is essential for mouse epiblast maturation through transcriptional and epigenetic control of Nodal signaling. eLife *6*, e33333.

Huang, J., Liu, X., Li, D., et al. (2016). Dynamic control of enhancer repertoires drives lineage and stage-specific transcription during hematopoiesis. Dev. Cell *36*, 9–23.

Hung, L.H., Heiner, M., Hui, J., et al. (2008). Diverse roles of hnRNP L in mammalian mRNA processing: a combined microarray and RNAi analysis. RNA *14*, 284–296.

Jalal, C., Uhlmann-Schiffler, H., and Stahl, H. (2007). Redundant role of DEAD box proteins p68 (Ddx5) and p72/p82 (Ddx17) in ribosome biogenesis and cell proliferation. Nucleic Acids Res. *35*, 3590–3601.

Jung, C., Mittler, G., Oswald, F., et al. (2013). RNA helicase Ddx5 and the noncoding RNA SRA act as coactivators in the Notch signaling pathway. Biochim. Biophys. Acta *1833*, 1180–1189.

Khan, A., Mathelier, A., and Zhang, X. (2018). Super-enhancers are transcriptionally more active and cell type-specific than stretch enhancers. Epigenetics *13*, 910–922.

Kim, D., Pertea, G., Trapnell, C., et al. (2013). TopHat2: accurate alignment of transcriptomes in the presence of insertions, deletions and gene fusions. Genome Biol. *14*, R36.

Klattenhoff, C.A., Scheuermann, J.C., Surface, L.E., et al. (2013). Braveheart, a long noncoding RNA required for cardiovascular lineage commitment. Cell *152*, 570–583.

Konermann, S., Brigham, M.D., Trevino, A.E., et al. (2015). Genome-scale transcriptional activation by an engineered CRISPR–Cas9 complex. Nature *517*, 583–588.

Langmead, B., and Salzberg, S.L. (2012). Fast gapped-read alignment with Bowtie 2. Nat. Methods *9*, 357–359.

Langmead, B., Trapnell, C., Pop, M., et al. (2009). Ultrafast and memory-efficient alignment of short DNA sequences to the human genome. Genome Biol. *10*, R25.

Larson, M.H., Gilbert, L.A., Wang, X., et al. (2013). CRISPR interference (CRISPRi) for sequence-specific control of gene expression. Nat. Protoc. *8*, 2180–2196.

Latos, P.A., Pauler, F.M., Koerner, M.V., et al. (2012). Airn transcriptional overlap, but not its lncRNA products, induces imprinted Igf2r silencing. Science *338*, 1469–1472.

Li, Z., Chao, T.C., Chang, K.Y., et al. (2014b). The long noncoding RNA THRIL regulates TNF expression through its interaction with hnRNPL. Proc. Natl Acad. Sci. USA *111*, 1002–1007.

Li, H., Lai, P., Jia, J., et al. (2017a). RNA helicase DDX5 inhibits reprogramming to pluripotency by miRNA-based repression of RYBP and its PRC1-dependent and -independent functions. Cell Stem Cell *20*, 571.

Li, W., Notani, D., and Rosenfeld, M.G. (2016). Enhancers as non-coding RNA transcription units: recent insights and future perspectives. Nat. Rev. Genet. *17*, 207–223.

Li, Y., Rivera, C.M., Ishll, H., et al. (2014a). CRISPR reveals a distal super-enhancer required for Sox2 expression in mouse embryonic stem cells. PLoS One *9*, e114485.

Li, X., Zhou, B., Chen, L., et al. (2017b). GRID-seq reveals the global RNA–chromatin interactome. Nat. Biotechnol. *35*, 940–950.

Lovén, J., Hoke, H.A., Lin, C.Y., et al. (2013). Selective inhibition of tumor oncogenes by disruption of super-enhancers. Cell *153*, 320–334.

Luo, S., Lu, J.Y., Liu, L., et al. (2016). Divergent lncRNAs regulate gene expression and lineage differentiation in pluripotent cells. Cell Stem Cell *18*, 637–652.

Micheletti, R., Plaisance, I., Abraham, B.J., et al. (2017). The long noncoding RNA Wisper controls cardiac fibrosis and remodeling. Sci. Transl. Med. *9*, eaai9118.

Moffat, J., Grueneberg, D.A., Yang, X., et al. (2006). A lentiviral RNAi library for human and mouse genes applied to an arrayed viral high-content screen. Cell *124*, 1283–1298.

Novo, C.L., Javierre, B.M., Cairns, J., et al. (2018). Long-range enhancer interactions are prevalent in mouse embryonic stem cells and are reorganized upon pluripotent state transition. Cell Rep. *22*, 2615–2627.

Okuda, A., Fukushima, A., Nishimoto, M., et al. (1998). UTF1, a novel transcriptional coactivator expressed in pluripotent embryonic stem cells and extra-embryonic cells. EMBO J. *17*, 2019–2032.

Ong, C.-T., and Corces, V.G. (2011). Enhancer function: new insights into the regulation of tissue-specific gene expression. Nat. Rev. Genet. *12*, 283–293.

Orom, U.A., Derrien, T., Beringer, M., et al. (2010). Long noncoding RNAs with enhancer-like function in human cells. Cell *143*, 46–58.

Ounzain, S., Micheletti, R., Arnan, C., et al. (2015). CARMEN, a human super enhancer-associated long noncoding RNA controlling cardiac specification, differentiation and homeostasis. J. Mol. Cell. Cardiol. *89*, 98–112.

Palikyras, S., and Papantonis, A. (2019). Modes of phase separation affecting chromatin regulation. Open Biol. *9*, 190167.

Rickels, R., and Shilatifard, A. (2018). Enhancer logic and mechanics in development and disease. Trends Cell Biol. *28*, 608–630.

Rinn, J.L., Kertesz, M., Wang, J.K., et al. (2007). Functional demarcation of active and silent chromatin domains in human HOX loci by noncoding RNAs. Cell *129*, 1311–1323.

Rossow, K.L., and Janknecht, R. (2003). Synergism between p68 RNA helicase and the transcriptional coactivators CBP and p300. Oncogene *22*, 151–156.

Sabari, B.R., Dall'Agnese, A., Boija, A., et al. (2018). Coactivator condensation at super-enhancers links phase separation and gene control. Science *361*, eaar3958.

Saporita, A.J., Chang, H.C., Winkeler, C.L., et al. (2011). RNA helicase DDX5 is a p53-independent target of ARF that participates in ribosome biogenesis. Cancer Res. *71*, 6708–6717.

Sauvageau, M., Goff, L.A., Lodato, S., et al. (2013). Multiple knockout mouse models reveal lincRNAs are required for life and brain development. eLife *2*, e01749.

Sengupta, D., Kannan, A., Kern, M., et al. (2015). Disruption of BRD4 at H3K27Ac-enriched enhancer region correlates with decreased c-Myc expression in Merkel cell carcinoma. Epigenetics *10*, 460–466.

Shechner, D.M., Hacisuleyman, E., Younger, S.T., et al. (2015). Multiplexable, locus-specific targeting of long RNAs with CRISPR-Display. Nat. Methods *12*, 664–670.

Shen, X., Liu, Y., Hsu, Y.J., et al. (2008). EZH1 mediates methylation on histone H3 lysine 27 and complements EZH2 in maintaining stem cell identity and executing pluripotency. Mol. Cell *32*, 491–502.

Shen, B., Zhang, J., Wu, H.Y., et al. (2013). Generation of gene-modified mice via Cas9/RNA-mediated gene targeting. Cell Res. *23*, 720–723.

Shin, S., and Janknecht, R. (2007). Concerted activation of the Mdm2 promoter by p72 RNA helicase and the coactivators p300 and P/CAF. J. Cell. Biochem. *101*, 1252–1265.

Shin, H.Y., Willi, M., Yoo, K.H., et al. (2016). Hierarchy within the mammary STAT5-driven Wap super-enhancer. Nat. Genet. *48*, 904–911.

Sun, Q., Hao, Q., and Prasanth, K.V. (2018). Nuclear long noncoding RNAs: key regulators of gene expression. Trends Genet. *34*, 142–157.

The ENCODE Project Consortium (2012). An integrated encyclopedia of DNA elements in the human genome. Nature *489*, 57–74.

Tilgner, H., Knowles, D.G., Johnson, R., et al. (2012). Deep sequencing of subcellular RNA fractions shows splicing to be predominantly co-transcriptional in the human genome but inefficient for lncRNAs. Genome Res. *22*, 1616–1625.

Trapnell, C., Roberts, A., Goff, L., et al. (2012). Differential gene and transcript expression analysis of RNA-seq experiments with TopHat and Cufflinks. Nat. Protoc. *7*, 562–578.

Wang, Z.X., Teh, C.H., Chan, C.M., et al. (2008). The transcription factor Zfp281 controls embryonic stem cell pluripotency by direct activation and repression of target genes. Stem Cells *26*, 2791–2799.

Werner, M.S., Sullivan, M.A., Shah, R.N., et al. (2017). Chromatin-enriched lncRNAs can act as cell-type specific activators of proximal gene transcription. Nat. Struct. Mol. Biol. *24*, 596–603.

Whyte, W.A., Orlando, D.A., Hnisz, D., et al. (2013). Master transcription factors and mediator establish super-enhancers at key cell identity genes. Cell *153*, 307–319.

Windbichler, N., and Schroeder, R. (2006). Isolation of specific RNA-binding proteins using the streptomycin-binding RNA aptamer. Nat. Protoc. *1*, 638–640.

Witte, S., Bradley, A., Enright, A.J., et al. (2015). High-density P300 enhancers control cell state transitions. BMC Genomics *16*, 903.

Wu, X., and Sharp, P.A. (2013). Divergent transcription: a driving force for new gene origination? Cell *155*, 990–996.

Xiang, J.F., Yin, Q.F., Chen, T., et al. (2014). Human colorectal cancer-specific CCAT1-L lncRNA regulates long-range chromatin interactions at the MYC locus. Cell Res. *24*, 513–531.

Yan, P., Luo, S., Lu, J.Y., et al. (2017). Cis- and trans-acting lncRNAs in pluripotency and reprogramming. Curr. Opin. Genet. Dev. *46*, 170–178.

Yang, Y.W., Flynn, R.A., Chen, Y., et al. (2014). Essential role of lncRNA binding for WDR5 maintenance of active chromatin and embryonic stem cell pluripotency. eLife *3*, e02046.

Yin, Y., Lu, J.Y., Zhang, X., et al. (2020). U1 snRNP regulates chromatin retention of noncoding RNAs. Nature *580*, 147–150.

Yin, Y., Yan, P., Lu, J., et al. (2015). Opposing roles for the lncRNA haunt and its genomic locus in regulating HOXA gene activation during embryonic stem cell differentiation. Cell Stem Cell *16*, 504–516.

Zhang, Y., Liu, T., Meyer, C.A., et al. (2008). Model-based analysis of ChIP-Seq (MACS). Genome Biol. *9*, R137.

Zhang, Y.E., Vibranovski, M.D., Landback, P., et al. (2010). Chromosomal redistribution of male-biased genes in mammalian evolution with two bursts of gene gain on the X chromosome. PLoS Biol. *8*, e1000494.

Zhang, Y., Wong, C.H., Birnbaum, R.Y., et al. (2013). Chromatin connectivity maps reveal dynamic promoter-enhancer long-range associations. Nature *504*, 306–310.

Zhao, Y., Zhou, J., He, L., et al. (2019). MyoD induced enhancer RNA interacts with hnRNPL to activate target gene transcription during myogenic differentiation. Nat. Commun. *10*, 5787.

Zhu, Y., Sun, L., Chen, Z., et al. (2013). Predicting enhancer transcription and activity from chromatin modifications. Nucleic Acids Res. *41*, 10032–10043.